Pergamon

Geochimica et Cosmochimica Acta, Vol. 68, No. 22, pp. 4595-4618, 2004

0016-7037/04 $30.00 + .00

doi:10.1016/j.gca.2004.05.023

Carbonatization of oceanic crust by the seafloor hydrothermal activity and its significance as a CO_2 sink in the Early Archean

KENTARO NAKAMURA* and YASUHIRO KATO

Department of Geosystem Engineering, University of Tokyo, 7-3-1 Hongo, Bunkyo-ku, Tokyo 113-8656 Japan

(*Received November* 6, 2003; *accepted in revised form May* 7, 2004)

Abstract—Early Archean (3.46 Ga) hydrothermally altered basaltic rocks exposed near Marble Bar, eastern Pilbara Craton, have been studied in order to reveal geological and geochemical natures of seafloor hydrothermal carbonatization and to estimate the CO_2 flux sunk into the altered oceanic crust by the carbonatization. The basaltic rocks are divided into basalt and dolerite, and the basalt is further subdivided into type I, having original igneous rock textures, and type II, lacking these textures due to strong hydrothermal alteration. Primary clinopyroxene phenocrysts are preserved in some part of the dolerite samples, and the alteration mineral assemblage of dolerite (chlorite + epidote + albite + quartz ± actinolite) indicates that the alteration condition was typical greenschist facies. In other samples, all primary minerals were completely replaced by secondary minerals, and the alteration mineral assemblage of the type I and type II basalts (chlorite + K-mica + quartz + carbonate minerals ± albite) is characterized by the presence of K-mica and carbonate minerals and the absence of Ca-Al silicate minerals such as epidote and actinolite, suggesting the alteration condition of high CO_2 fugacity. The difference of the alteration mineral assemblages between basalt and dolerite is probably attributed to the difference of water/rock ratio that, in turn, depends on their porosity.

Carbonate minerals in the carbonatized basalt include calcite, ankerite, and siderite, but calcite is quite dominant. The $\delta^{13}C$ values of the carbonate minerals are $-0.3 \pm 1.2‰$ and mostly within the range of marine carbonate, indicating that the carbonate minerals were formed by seafloor hydrothermal alteration and that carbonate carbon in the altered basalt was derived from seawater. Whole-rock chemical composition of the basaltic rocks is essentially similar to that of modern mid-ocean ridge basalt (MORB) except for highly mobile elements such as K_2O, Rb, Sr, and Ba. Compared to the least altered dolerite, all altered basalt samples are enriched in K_2O, Rb, and Ba, and are depleted in Na_2O, reflecting the presence of K-mica replacing primary plagioclase. In addition, noticeable CO_2 enrichment is recognized in the basalt due to the ubiquitous presence of carbonate minerals, but there was essentially neither gain nor loss of CaO. This suggests that the CO_2 in the hydrothermal fluid (seawater) was trapped by using Ca originally contained in the basalt. The CaO/CO_2 ratios of the basalt are generally the same as that of pure calcite, indicating that Ca in the basalt was almost completely converted to calcite during the carbonatization, although Mg and Fe were mainly redistributed into noncarbonate minerals such as chlorite.

The carbon flux into the Early Archean oceanic crust by the seafloor hydrothermal carbonatization is estimated to be 3.8×10^{13} mol/yr, based on the average carbon content of altered oceanic crust of 1.4×10^{-3} mol/g, the alteration depth of 500 m, and the spreading rate of 1.8×10^{11} cm^2/yr. This flux is equivalent to or greater than the present-day total carbon flux. It is most likely that the seafloor hydrothermal carbonatization played an important role as a sink of atmospheric and oceanic CO_2 in the Early Archean.

1. INTRODUCTION

Carbonate minerals are well known as the largest carbon reservoir in the Earth's surface (e.g., Ronov and Yaroshevsky, 1967; Ronov and Yaroshevsky 1969; Holland, 1984), and their precipitation plays a key role as a CO_2 sink in the atmosphere and ocean (Walker et al., 1981; Berner et al., 1983; Berner, 1991). Therefore, the style of carbonate precipitation and its flux are considered to be among critical factors determining atmospheric and oceanic CO_2 levels. It is commonly assumed that carbonate minerals mainly precipitate as sedimentary carbonates by the reaction between bicarbonate ions in seawater and some cations (Ca^{2+}, Mg^{2+}, Fe^{2+}, Mn^{2+}) mostly derived from weathered continental crust in the modern Earth (Walker et al., 1981; Berner et al., 1983). This reaction is mostly driven by biogenic activity of coral, foraminifera, and coccoliths. Besides the biogenic activity, Walker et al. (1981) pointed out that the carbonate precipitation flux is substantially controlled by the continental weathering rate. On the other hand, the style and flux of carbonate precipitation in the Archean Earth are still uncertain. Further, the Archean atmospheric CO_2 level has been hotly debated in the past several years. It has been long believed that the atmospheric CO_2 level in the Archean was much higher than today, and the CO_2 greenhouse effect compensated for the faint solar luminosity of the young sun (Kasting, 1987; Tajika and Matsui, 1992; Kasting 1993). However, Rye et al. (1995) suggested that the 2.2 to 2.75 Ga atmospheric CO_2 concentration was at least five times lower than that required in one-dimensional climate models to compensate for lower solar luminosity at that time, based on geochemical data from paleosols. Quite recently, Kasting and his colleagues discarded the previous model by Kasting (1993) and postulated that the greenhouse effect by CH_4 was more important than

* Author to whom correspondence should be addressed (tkentaro@mail.ecc.u-tokyo.ac.jp).

previously thought, and the atmospheric CO_2 level during the Middle to Late Archean was not so high (Pavlov et al., 2000).

In the Archean Cratons, the quantity of sedimentary carbonates is quite small (Ronov, 1964; Veizer et al., 1989). Alternatively, hydrothermally carbonatized greenstones have been widely recognized in the Archean volcanic successions (e.g., Barley, 1993; de Wit and Hart, 1993). The Archean hydrothermal carbonatization has been classified into two types on the basis of geological, mineralogical, and carbon isotopic features; fault-related carbonatization and regional carbonatization (e.g., Barley and Groves, 1987; Groves et al., 1988; Veizer et al., 1989). The former type mostly occurs along large faults and shear zones. The carbonatized greenstones of this type commonly contain Mg-rich carbonate minerals such as dolomite and magnesite (Groves et al., 1988; Veizer et al., 1989). Carbon isotope ratios ($\delta^{13}C$) of the carbonate minerals are around $-4‰$, so this type of carbonatization is attributed to a mantle degassing (e.g., Burrows et al., 1986; Cameron and Hattori, 1987; Golding et al., 1987; Groves et al., 1988). On the other hand, the latter type of carbonatization is not spatially or temporally related to these large faults and shear zones. The greenstones that have suffered from this type of carbonatization are extensively distributed throughout the greenstone belts. The carbonate mineral assemblage is calcite + ankerite ± siderite (Groves et al., 1988; Veizer et al., 1989). This carbonatization is generally considered to have been attributed to seafloor hydrothermal activity, because the $\delta^{13}C$ values of the carbonate minerals are close to $0‰$, suggesting derivation from seawater (e.g., Barley and Groves, 1987; Groves et al., 1988; Barley, 1993).

In the past couple of decades, studies have focused on the fault-related carbonatization because this type is closely related to gold mineralization (e.g., Burrows et al., 1986; Phillips, 1986; Cameron and Hattori, 1987; Groves et al., 1988). However, understanding the seafloor hydrothermal carbonatization is very important for giving some constraints on the global carbon cycle and environmental changes of the Archean Earth's surface. In the present paper, we report petrological and geochemical features of seafloor hydrothermally carbonatized greenstones from the Salgash Subgroup (upper part of the Warrawoona Group), Pilbara Craton, and try to estimate the carbon flux sunk into the Early Archean oceanic crust.

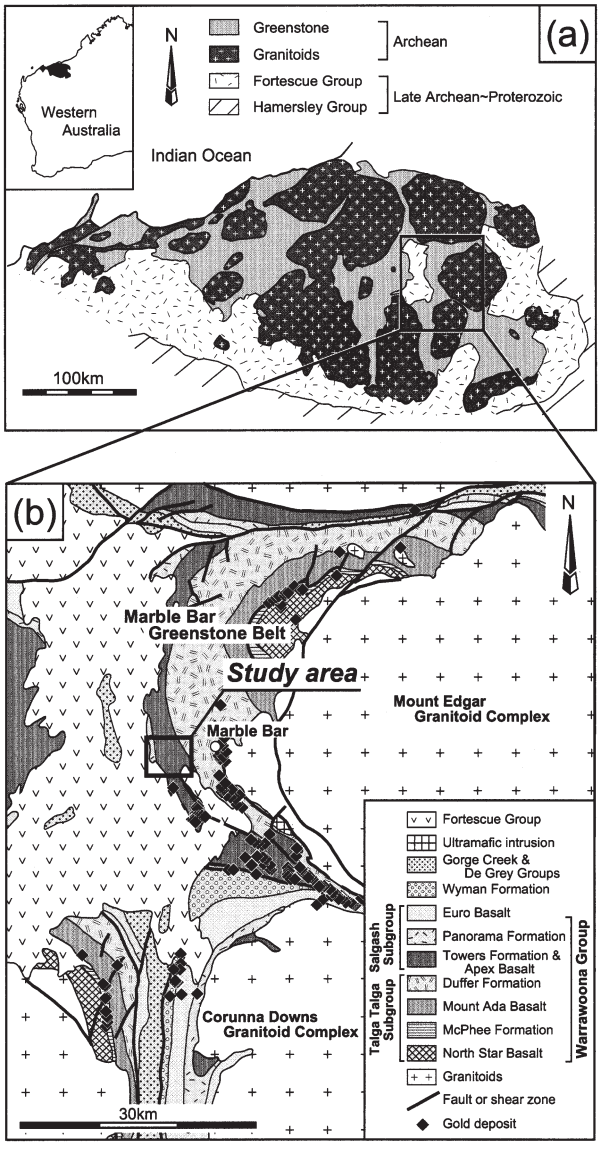

Fig. 1. Geological map of (a) the Pilbara Craton (after Hickman (1983)) and (b) the eastern Pilbara region (after Van Kranendonk et al. (2001)) showing the location of hydrothermal gold deposits (Ferguson and Ruddock, 2001).

2. GEOLOGICAL SETTING

The Pilbara Craton consists of the Early to Late Archean granitoid-greenstone terrane, which is unconformably overlain by volcano-sedimentary sequences of the Late Archean to Early Proterozoic Hamersley Group (Hickman, 1983; Arndt et al., 1991). The granitoid-greenstone terrane is characterized by an ovoid pattern of granitoid/gneiss batholiths and enveloping greenstones (Fig. 1a). The greenstones are composed mainly of ultramafic to mafic volcanic rocks with significant amounts of intermediate to felsic volcanic rocks and sediments. This craton has been considered to retain a substantial portion of the most pristine Archean greenstone successions in the world (Barley, 1993; de Wit and Hart, 1993).

The study area of the present contribution is located in the eastern Pilbara Craton, approximately 5 to 10 km west of the Marble Bar town (Fig. 1b). Greenstones belonging to the Warrawoona Group (the Talga Talga Subgroup and Salgash Subgroup in ascending stratigraphic order) are extensively exposed in this area. The Talga Talga Subgroup comprises tholeiite/komatiite successions of the North Star Basalt, McPhee Formation, and Mount Ada Basalt and calc-alkaline volcanic suites of the Duffer Formation. The Salgash Subgroup is also composed of tholeiite/komatiite successions of the Towers Formation, Apex Basalt, and Euro Basalt and calc-alkaline volcanic suites of the Panorama Formation. It has been generally accepted that the calc-alkaline volcanic rocks are a product of island-arc or continental margin-arc volcanism (e.g., Barley and Pickard, 1999), but the tectonic setting of the tholeiite/komatiite successions is still controversial. Barley (1993) interpreted that geological and petrological characteristics of the Warrawoona basalt are comparable to those developed in

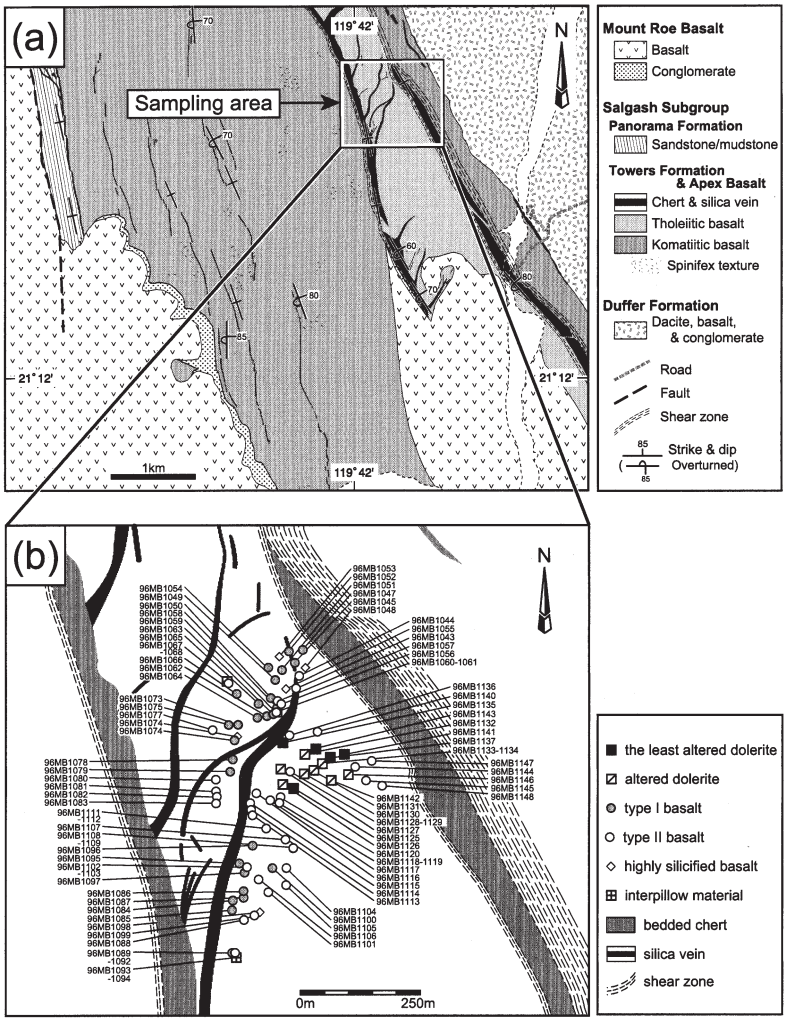

Fig. 2. (a) Geological map of the study area (after Kato and Nakamura (2003)) and (b) locality map showing distribution of each rock type.

younger volcanic-arc or near-arc settings, although some geochemical features of the tholeiitic basalt are similar to those of modern mid-ocean ridge basalt (MORB). Green et al. (2000) reported that the tholeiitic/komatiitic basalts of the Warrawoona Group in the Pilgangoora Greenstone Belt assimilated up to 25% crustal material, and then concluded that the basalts were erupted onto continental basement, not onto the ocean floor. On the other hand, Condie (1997) pointed out that the chemical features of the Warrawoona basalts are similar to those of modern oceanic plateaus. Barley and Pickard (1999) also interpreted that the tholeiite/komatiite assemblage most likely formed in oceanic plateau or marginal basin settings. Maruyama et al. (1991), however, asserted that the greenstones in the Talga Talga Subgroup are a remnant of oceanic crust accreted to the island-arc or continental margin arc based on the reconstruction of oceanic plate stratigraphy and the recognition of duplex structure. Very recently, Kato and Nakamura (2003) demonstrated that the tholeiitic and komatiitic basalt units in the Marble Bar Greenstone Belt were deposited in a mid-oceanic spreading center and a hot spot, respectively, based on the geological mapping and geochemical analyses of basaltic rocks and associated hydrothermal bedded cherts.

A geological map of the study area is shown in Figure 2a (Kato and Nakamura, 2003). This area is isolated from the shear zones associated with hydrothermal gold deposits (Fig. 1b; Ferguson and Ruddock, 2001). Therefore, the influence of the fault-related alteration of later stage is expected to be negligible in this study area. The Towers Formation and Apex Basalt that are composed mainly of pillowed basalt with minor massive basaltic rocks and intercalated bedded cherts are extensively exposed in the central part of the study area (Fig. 2a). Pillow shapes indicate a stratigraphic facing "top to the west" without exception. The Duffer Formation that is dominated by dacite and conglomerate occurs in the eastern part, and the Panorama Formation that is composed of a thick alternation of sandstone and mudstone overlies the Apex Basalt in the western part. The Mount Roe Basalt (ca. 2770 Ma) unconformably overlies the Salgash Subgroup with a basal conglomerate and is separated from the Panorama Formation by an N-S trending high-angle normal fault.

Depositional age of the basalt/chert units of the Towers Formation and Apex Basalt is regarded as between 3463 and 3454 Ma on the basis of zircon U-Pb ages of the underlying Duffer Formation (Thorpe et al., 1992; McNaughton et al., 1993) and overlying Panorama Formation (Thorpe et al., 1992). The basalt/chert units are divided into tholeiitic basalt and komatiitic basalt units (Kato and Nakamura, 2003). The tholeiitic basalt is a Fe-rich, low-K tholeiite. It is conformably overlain by a thick bedded chert (~13 m) and is crosscut by well-developed (500m long and 10m wide) black/gray massive silica veins. These silica veins intersect the overlying bedded chert at the base of the bedded chert, but never penetrate it. The komatiitic basalt has relatively high-MgO content, and small pyroxene spinifex texture (up to 10mm long) is locally observed in the massive lava. The komatiitic basalt is overlain by thin (<6 m) bedded cherts. The black/gray massive silica veins in this unit are small-scale (<100 m long and several decimeters wide) and are not developed well.

The tectonic setting of the tholeiitic basalt unit (the target of the present study) has been discussed in Kato and Nakamura (2003) and their results are summarized as follows:

1. MORB-normalized trace element patterns and chondrite-normalized rare earth element (REE) patterns indicate that the tholeiitic basalt is MORB in origin. Moreover, the tholeiitic basalt plots within the region of N-MORB on the Th-Hf-Ta and Zr-Nb-Y discrimination diagrams.
2. Although some other greenstones in the Warrawoona and Coonterunah Groups are contaminated by crustal material (Condie, 1994; Green et al., 2000), geochemical features of the tholeiitic basalt clearly indicate considerably low or no crustal contamination.
3. Geochemical features of bedded cherts associated with the tholeiitic basalt are similar to those of modern hydrothermal Fe-rich sediments at the MOR.
4. The absence of continental detritus in these bedded cherts also indicates that their depositional site was truly oceanic and remote from a continent or island-arcs composed of felsic plutonic/volcanic rocks.
5. The massive silica veins associated with the bedded cherts were hydrothermal feeders producing these cherts on the seafloor, emplaced up normal fault zones in the MOR.
6. The tholeiitic basalt unit (the lowermost of the Apex Basalt) has a tectonic contact with the underlying felsic succession (Duffer Formation), suggesting that the Duffer Formation and Apex Basalt were not deposited continuously.

Consequently, these geochemical and geological lines of evidence consistently indicate that the tholeiitic basalt unit is a remnant of oceanic crust.

The tholeiitic basalt was generally subject to hydrothermal alteration, including carbonatization and silicification. In particular, the strongly altered basalt occurs below the hydrothermal bedded cherts and in the vicinity of the massive silica veins, suggesting that seafloor hydrothermal activity is responsible for the basalt alteration. Detailed sampling of basaltic rocks was performed in the tholeiitic basalt unit that is interpreted as a remnant of oceanic crust (Fig. 2a). We collected 93 samples from almost all outcrops in this area.

3. SAMPLE DESCRIPTION

The collected samples are divided into two types on the basis of field occurrences and microscopic characteristics; basalt and dolerite. The basalt is further subdivided into type I with primary igneous rock textures, and type II without them. In addition, five samples are characterized by highly silicified alteration. Five samples from interpillow space that is filled with carbonate minerals, quartz, and completely altered rock fragments were also selected. Sampling localities are shown in Figure 2b. A detailed description of each lithology is given below.

3.1. Dolerite

Dolerite occurs as a massive lava in the stratigraphically lower part (more than 300m from the base of overlying bedded chert) of the tholeiitic basalt unit (Fig. 2b). In our mapped area, the massive dolerite is a significantly minor component. The dolerite exhibits a holocrystalline ophitic texture (Fig. 3a) and is greenish in color due to the presence of chlorite and epidote. Microscopic observation indicates that the least altered dolerite samples ($n = 5$) have primary clinopyroxene phenocrysts, but other dolerite samples lack them. In the least altered dolerite, subhedral to anhedral primary clinopyroxene phenocrysts survive hydrothermal alteration, and there is no alteration mineral vein (Fig. 3a). On the other hand, all primary phases in the altered dolerite are completely replaced by secondary phases. Veinlets and vesicles filled with alteration minerals are locally observed in these samples. The alteration mineral assemblage of the dolerite is chlorite + epidote + albite + quartz ± actinolite, indicating the alteration condition of typical greenschist facies.

Clinopyroxene phenocrysts are partly or completely replaced by chlorite, and the edges of the phenocrysts are sometimes replaced by actinolite needles. Plagioclase phenocrysts are completely replaced by epidote, albite, and quartz. Veinlets and vesicles are generally filled with microcrystalline quartz aggregates, and epidote veinlets rarely occur. Pyrite is disseminated as an opaque mineral. In a few altered dolerite samples, trace amounts of K-mica and carbonate minerals replace plagioclase phenocrysts, and carbonate minerals fill vesicles.

3.2. Type I Basalt

Type I basalt exclusively occurs as a pillowed lava. It is variable in color (greenish, whitish, and light reddish), probably reflecting the degree of alteration. Hyalo-ophitic and intersertal textures are well preserved as a primary igneous rock texture (Fig. 3b), but primary minerals are completely replaced by secondary minerals. Pseudomorphs after olivine phenocrysts and plagioclase laths are commonly recognized (Fig. 3b). The alteration mineral assemblage is chlorite + K-mica + quartz + carbonate minerals ± albite, which is quite different from that of the dolerite.

Olivine phenocrysts are completely replaced by chlorite, carbonate minerals, and quartz. All plagioclase phenocrysts and laths are replaced by K-mica, quartz, carbonate minerals, and albite. Groundmass is replaced by chlorite, carbonate minerals, and fine-grained opaque minerals (Fig. 3c). Some parts of

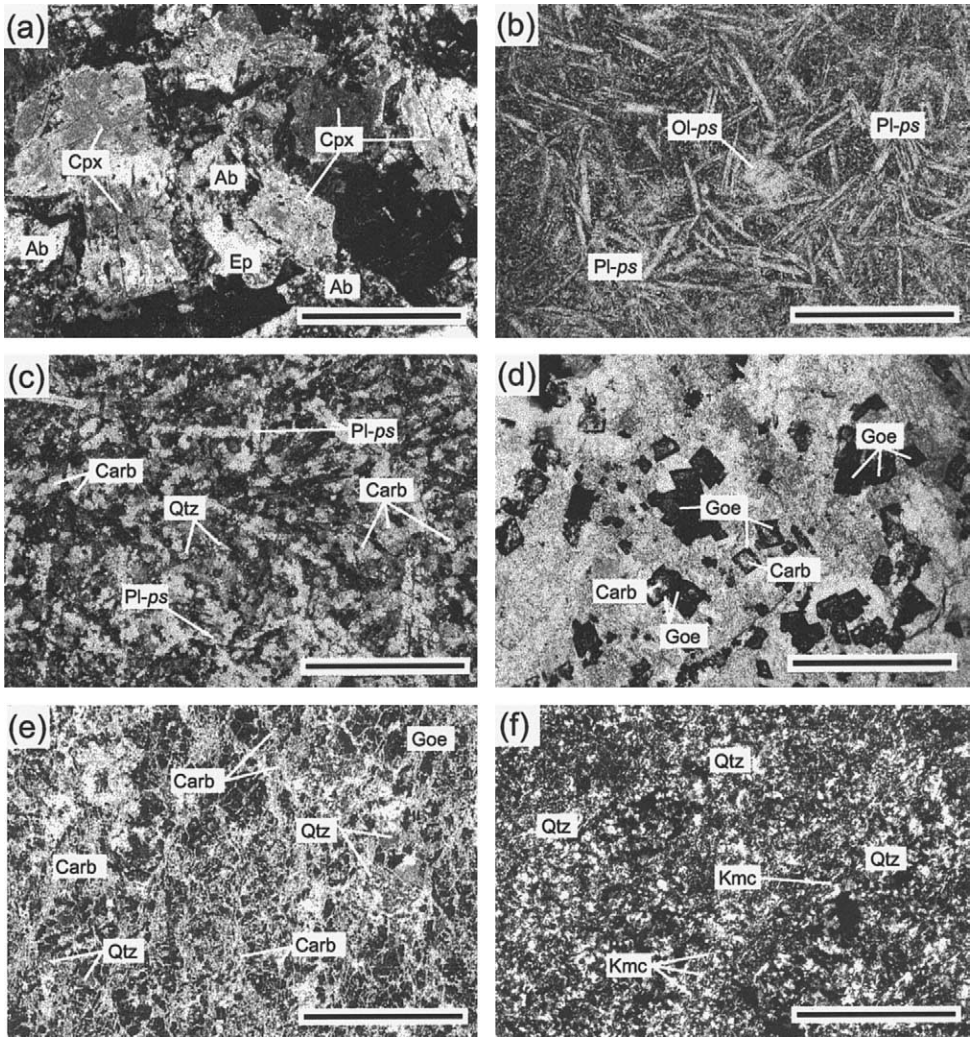

Fig. 3. Photomicrographs of dolerite and basalt samples: (a) Primary clinopyroxene phenocrysts with holocrystalline ophitic texture in the least altered dolerite; (b) pseudomorphs after olivine phenocrysts and plagioclase laths in the type I basalt; (c) carbonate minerals scattered in groundmass of the type I basalt; (d) rhombic siderite partly replaced by goethite in the type I basalt; (e) carbonate mineral networks in the type II basalt; and (f) fine quartz grains and K-mica blades in the highly silicified basalt. Mineral abbreviations: Ol-*ps* = olivine pseudomorphed by chlorite, quartz, and carbonate; Pl-*ps* = plagioclase pseudomorphed by K-mica, quartz, and carbonate; Cpx = clinopyroxene; Ep = epidote; Ab = albite; Qtz = quartz; Carb = carbonate minerals; Kmc = K-mica; Goe = goethite. Scale bar: 1mm (b, c, e, f), 0.4mm (a, d).

carbonate minerals disseminated in groundmass have a rhombic shape (Fig. 3d). Veinlets filled with fibrous K-mica and quartz generally occur. Carbonate minerals filling veinlets and vesicles are rare in the type I compared to the type II. Pyrite is sometimes observed in groundmass as an opaque mineral. Very fine-grained goethite partly or completely replaces Fe-rich carbonate mineral and pyrite in some samples (Fig. 3d), which is probably the product of modern weathering. However, Fe-rich carbonate mineral and pyrite commonly survive the replacement by goethite, suggesting that the modern weathering is not so intense as to change primary petrological and geochemical signatures of our samples.

3.3. Type II Basalt

Type II basalt occurs as a pillowed lava and has greenish, whitish, and light reddish colors. Primary igneous rock textures are quite unclear because these rocks were subject to intense hydrothermal alteration. The alteration mineral assemblage of the type II (chlorite + K-mica + quartz + carbonate minerals) is essentially the same as that of the type I.

Chlorite is the dominant secondary phase. Pseudomorphs after primary mafic minerals, including olivine and clinopyroxene, are not recognizable. Carbonate minerals mainly fill veinlets and vesicles (Fig. 3e). All carbonate veinlets and vesicles are microscopic and completely different in mode of occurrence from carbonate veins in the modern oceanic crust. Quartz also fills veinlets and vesicles with or without carbonate minerals. K-mica occurs as needles and aggregates, and some of the K-mica aggregates are recognized as pseudomorphs after plagioclase. Opaque minerals that are mainly pyrite and goethite pseudomorph after pyrite are generally observable. The type II basalt is characterized by a significant amount of vein-

lets and common pyrite (or goethite pseudomorph), implying that these rocks suffered from intense hydrothermal alteration.

3.4. Highly Silicified Basalt and Interpillow Material

Five highly silicified basalt samples are composed chiefly of quartz and K-mica (Fig. 3f). Many veins and vesicles filled with quartz are recognized in these samples. K-mica replaces plagioclase laths and occurs as fibers intergrown with quartz grains in veinlets and vesicles. Pyrite and goethite pseudomorphs after pyrite are observable in quartz veins.

Interpillow spaces are commonly filled with carbonate minerals, quartz, and small rock fragments. The rock fragments are strongly altered and completely replaced by secondary minerals such as chlorite, K-mica, and carbonate minerals. Pyrite and goethite after pyrite locally occur in the interpillow space.

4. ANALYTICAL METHODS

Chemical compositions of carbonate minerals were determined by JEOL JXA-733 electron probe X-ray microanalyzer (EPMA) at the Ocean Research Institute, University of Tokyo. Accelerating voltage and beam current are 15 kV and 7nA, respectively. Whole-rock chemical analyses were performed by using the techniques of Kato et al. (1998) and Kato et al. (2002). Powders for the whole-rock chemical analyses were prepared from rock samples sawed into slabs free of weathered surface, polished off saw marks, ultrasonicated in deionized water, chipped into small pieces in an agate mortar, and then pulverized in an agate ball mill. Microscopic veinlets and vesicles are included in the whole-rock powders. Loss on ignition (LOI) was calculated by igniting rock powders at 950°C for 6 h. Ignited rock powders were well mixed with $Li_2B_4O_7$ flux in exact ratio of 0.4000:4.0000 g and fused at 1150 to 1170°C for 7 min in a Pt crucible. Major element analysis of whole-rock samples was accomplished by Rigaku 3270 X-ray fluorescence (XRF) on fused glass bead at the Ocean Research Institute, University of Tokyo. CO_2 concentrations were determined by using LECO CNS-2000 Carbon, Nitrogen, and Sulfur determinator at the Department of Earth and Planetary Sciences, University of Tokyo. Trace and rare earth element concentrations were obtained by Yokogawa Analytical Systems PMS-200 inductively coupled plasma mass spectrometry (ICP-MS) at the Geological Survey of Japan. Rock powders (0.1000 g) were completely dissolved by HNO_3-$HClO_4$-HF digestion in a tightly sealed 7mL Teflon PFA screw-cap beaker, heated for 24 h over a hot plate at under 180°C, then evaporated to dryness. The residue was dissolved with 5 mL (1 + 1) HNO_3 by heating, and this solution was diluted to a factor of 1000 in mass. Measurements were separately performed for the trace elements with lighter mass numbers (Sc, V, Cr, Co, Ni, Cu, Zn, Rb, Sr, Y, Zr, Nb, and Ba) and for the REEs (La, Ce, Pr, Nd, Sm, Eu, Tb, Dy, Ho, Er, Tm, Yb, and Lu) together with four heavier trace elements (Hf, Ta, Th, and U) to gain maximum sensitivity and stability. The determination of lighter trace elements was obtained by using the standard addition method. More details of ICP-MS measurement, including operation conditions, are given in Imai (1990). REE data of the Leedey chondrite standard obtained by Masuda et al. (1973) and Masuda (1975) are used as normalization values in this paper. Carbon isotope analysis was conducted at the Central Research Institute, Mitsubishi Materials Corporation by using Micromass Optima Isotope Ratio Mass Spectrometer. The extraction of CO_2 from whole-rock samples was done using anhydrous phosphoric acid in sealed vessels. All values are reported with δ notation in per mil (‰) with reference to PDB (PeeDee Belemnite limestone) standard. The precision and accuracy of the isotope analysis are estimated to be better than 0.2 ‰.

5. RESULTS

5.1. Carbonate Mineral Chemistry

Based on EPMA analysis, it is recognized that carbonate minerals in the altered basalt are calcite, ankerite, and siderite (Fig. 4). Dolomite and magnesite are absent. The carbonate mineral replacing plagioclase is only calcite (Fig. 4a). On the other hand, the carbonate minerals replacing mafic minerals and glass are calcite, ankerite, and siderite (Fig. 4b). This suggests that Fe and Mg in the primary mafic minerals and glass are redistributed partly into ankerite and siderite during the hydrothermal alteration. The carbonate minerals filling veinlets and vesicles are mostly calcite with minor ankerite (Fig. 4c). Interpillow space is filled with calcite and siderite (Fig. 4d) and ankerite is not recognized.

The carbonate minerals contain some amounts of MnO (Fig. 5). The MnO concentration of siderite is less than 0.5 wt.%, and that of ankerite is higher than siderite, up to 1.5 wt.%. The calcites replacing primary minerals and filling veinlets have about the same MnO contents as ankerite, whereas the MnO content of interpillow-filling calcite is much greater (3 wt.% at maximum).

5.2. Carbon Isotopic Composition

Stable carbon isotope analysis of 42 whole-rock carbonate samples (2 altered dolerites, 17 type I basalts, 20 type II basalts, and 3 interpillow materials) that contain enough carbonate carbon to determine carbon isotopes was carried out. The $\delta^{13}C$ values expressed as a per mil deviation from the PDB reference scale are presented in Table 1, and average $\delta^{13}C$ values of each lithology are listed in Table 2. All the samples have a quite narrow range of $\delta^{13}C$ from −3.4 to 1.9‰ and the average $\delta^{13}C$ value is close to zero (average: −0.3‰, standard deviation: 1.2‰). As shown in Figure 6 in more detail, $\delta^{13}C$ values of carbonate minerals in altered dolerite are −1.8‰ and −1.4‰. The average values ($\pm 1\sigma$) of type I and type II basalts are −0.1 ± 1.1‰ and −0.4 ± 1.3‰, respectively. The interpillow carbonate minerals have the average $\delta^{13}C$ value of 0.0‰.

5.3. Whole-Rock Geochemistry

Major, trace, and rare earth element contents of dolerite, type I basalt, type II basalt, highly silicified basalt, and interpillow material are listed in Table 1. Average chemical compositions with ranges and standard deviations of each lithology are given in Table 2.

The dolerite samples have 49.52 wt.% SiO_2 on average. This SiO_2 value is within the typical range of basaltic rock. The average contents of CaO, Na_2O, and K_2O are 10.54, 2.13, and 0.27 wt.%, respectively. These oxide concentrations of the dolerite are relatively the same as those of modern MORB. The average CO_2 content is relatively low (0.72 wt.%) and LOI content is slightly high (3.86 wt.%), reflecting the ubiquitous presence of hydrous alteration minerals such as chlorite and epidote in the dolerite.

The type I basalt has the slightly high average SiO_2 content of 56.89 wt.% and exhibits a relatively wide range (46.76–65.37 wt.%). The average CaO content is relatively low (4.97 wt.%), whereas the range of CaO content is wide (0.12–12.45 wt.%). The Na_2O concentration (avg = 0.52 wt.%, range = 0–1.90 wt.%) is much lower than that of dolerite (avg = 2.13 wt.%, range = 1.58–2.91 wt.%), and the K_2O concentration (avg = 0.66 wt.%, range = 0.04–2.66 wt.%) is significantly higher than that of dolerite (avg = 0.27 wt.%, range = 0.04–

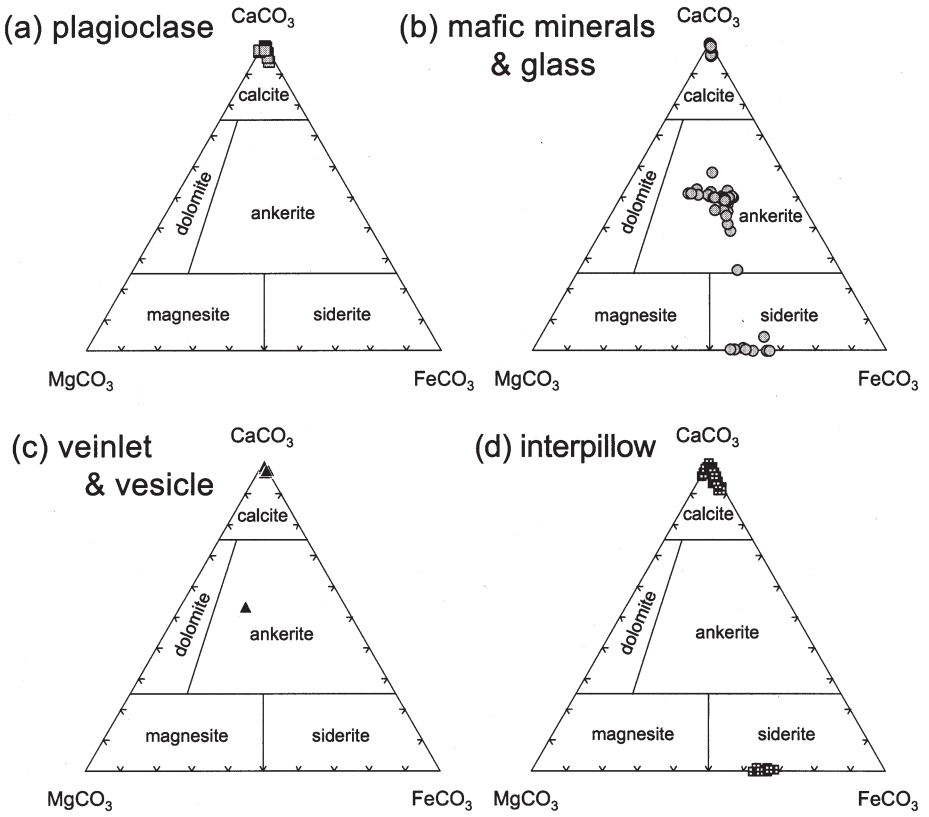

Fig. 4. Classification of carbonate minerals on the $CaCO_3$-$MgCO_3$-$FeCO_3$ diagram: (a) Carbonate minerals replacing plagioclase; (b) carbonate minerals replacing mafic minerals and glass; (c) carbonate minerals in veinlets and vesicles; and (d) carbonate minerals in interpillow space.

1.01 wt.%). The CO_2 content (avg = 4.43 wt.%, range = 0.01–12.93 wt.%) is significantly higher than that of dolerite (avg = 0.72 wt.%, range = 0.03–3.82 wt.%).

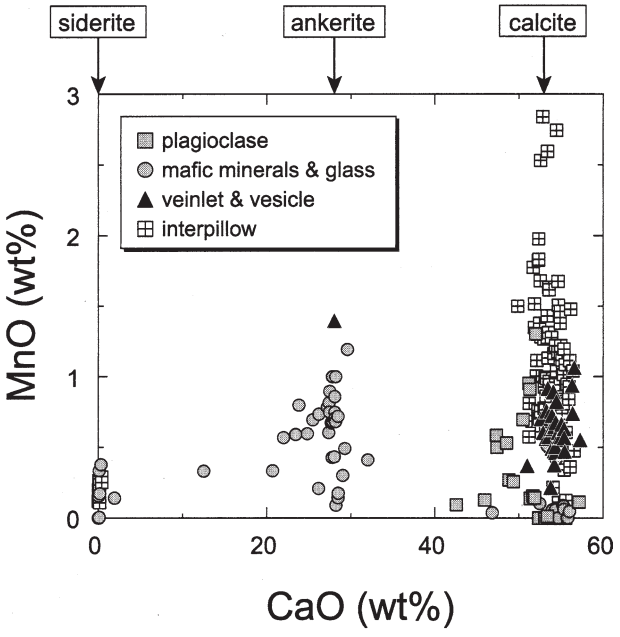

Fig. 5. CaO vs. MnO for carbonate minerals.

The average SiO_2 concentration of type II basalt (51.32 wt.%) is within typical basaltic abundance, although the SiO_2 range of this type is wide (30.70–65.69 wt.%). The average CaO content is 10.52 wt.%, which is essentially the same as that of dolerite, but the range of CaO is extremely wide (0.07–40.15 wt.%). The average Na_2O concentration of type II basalt (0.28 wt.%) is much lower than that of dolerite (2.13 wt.%). In contrast, the K_2O concentration (avg = 1.29 wt.%, range = 0–3.86 wt.%) is noticeably higher than that of dolerite (avg = 0.27 wt.%, range = 0.04–1.01 wt.%). The average CO_2 content (8.17 wt.%) is remarkably higher than that of dolerite (0.72 wt.%), while the CO_2 content widely ranges from 0.01 to 27.99 wt.%.

Highly silicified samples have high SiO_2 and K_2O contents (83.00 and 2.80 wt.% on average, respectively), reflecting the ubiquity of quartz and K-mica. In compensation for the high SiO_2 abundance, other major element concentrations are significantly lower than those of dolerite.

The incompatible trace element characteristics of dolerite and basalt can be portrayed using multielement plots normalized to modern MORB (Fig. 7). Except for Rb, Ba, K, and Sr, dolerite and basalt exhibit flat patterns, and their elemental abundances are generally the same as those of modern MORB. These latter elements are generally regarded to be immobile during alteration. This suggests that the primary compositions of these rocks are quite similar to those of modern MORB. On the other hand, Rb, Ba, and K

Table 1. Major, trace, and rare earth element data.

Lithology	Dolerite												
Rock type	The least altered					Altered							
Sample No.	96MB1125	96MB1135	96MB1137	96MB1141	96MB1143	96MB1126	96MB1127	96MB1130	96MB1131	96MB1132	96MB1134	96MB1142	96MB1146
SiO_2 (wt%)	51.27	49.33	47.40	48.15	49.49	49.56	52.29	50.48	49.58	49.10	47.93	49.66	49.49
TiO_2	0.98	0.67	0.61	0.68	0.66	0.82	0.87	0.58	0.64	0.65	0.69	0.64	0.65
Al_2O_3	14.0	17.1	16.0	15.2	15.7	16.5	16.1	14.8	16.3	16.3	16.3	16.2	17.1
Fe_2O_3t	13.32	10.60	12.04	12.48	11.80	13.77	11.46	12.26	11.05	11.25	11.71	10.10	10.43
MnO	0.192	0.157	0.182	0.173	0.173	0.202	0.172	0.183	0.160	0.163	0.168	0.161	0.154
MgO	7.04	7.64	12.33	11.64	7.86	8.20	7.85	9.24	7.99	8.10	8.06	8.15	7.26
CaO	10.96	11.69	9.24	9.22	12.31	7.24	7.04	10.33	10.80	11.51	13.07	11.77	11.80
Na_2O	1.94	2.34	1.61	1.62	1.76	2.84	2.23	1.58	2.91	2.37	1.61	2.09	2.76
K_2O	0.11	0.13	0.26	0.25	0.10	0.22	1.01	0.04	0.13	0.17	0.09	0.84	0.14
P_2O_5	0.067	0.046	0.052	0.047	0.044	0.052	0.057	0.045	0.039	0.046	0.048	0.040	0.047
Total	99.85	99.74	99.73	99.50	99.86	99.37	99.08	99.57	99.63	99.64	99.65	99.62	99.84
LOI	2.67	2.88	4.44	4.11	3.77	3.60	7.93	6.03	2.95	3.45	2.75	2.81	2.84
CO_2	nd	0.09	nd	0.12	0.92	0.06	3.82	2.22	0.03	0.49	0.03	0.04	0.05
Sc (ppm)	42.0	33.2	35.0	29.7	35.4	77.6	31.6	47.7	42.6	41.9	37.7	40.1	39.9
V	305	224	276	265	236	582	227	292	283	256	224	282	265
Cr	12.9	416	218	143	493	101	114	691	467	490	453	597	543
Co	48.4	49.6	113	77.5	65.3	103	41.8	59.5	60.2	57.9	53.1	53.8	66.2
Ni	67.7	139	571	410	211	104	76.3	186	151	173	160	132	152
Cu	166	104	173	119	161	112	120	189	188	171	151	164	200
Zn	74.1	88.3	131	78.1	79.6	140	68.1	79.8	68.2	109	72.0	78.6	81.6
Rb	3.1	4.8	8.4	8.1	3.0	8.4	26.6	2.1	3.9	4.4	2.0	27.3	5.1
Sr	188	148	95.8	90.5	125	201	54.1	120	129	148	174	127	149
Y	17.7	11.9	13.6	12.6	11.6	21.9	12.8	14.4	12.0	12.2	13.9	13.7	13.5
Zr	46.2	29.8	36.8	35.4	30.1	49.3	37.5	34.0	29.8	33.1	35.6	29.9	35.0
Nb	2.25	1.28	1.71	1.41	1.42	2.13	1.55	1.70	1.29	1.53	1.60	1.22	1.25
Mo	0.36	0.21	0.15	0.06	0.52	0.12	0.10	0.06	0.12	0.12	0.20	0.14	0.22
Ba	69	47	46	51	24	110	315	34	47	31	30	235	45
Hf	1.39	0.92	0.99	0.97	0.76	1.13	1.18	0.88	0.77	0.90	0.94	0.84	0.91
Ta	0.20	0.14	0.12	0.13	0.11	0.86	0.15	0.12	0.09	0.11	0.11	0.10	0.11
Th	0.28	0.19	0.20	0.19	0.16	0.22	0.24	0.17	0.16	0.17	0.19	0.23	0.18
U	0.06	0.05	0.05	0.05	0.05	0.04	0.07	0.05	0.05	0.03	0.03	0.05	0.05
La (ppm)	2.90	1.95	1.97	1.88	1.96	2.53	2.97	1.79	1.70	1.88	2.39	1.79	2.03
Ce	7.40	5.15	5.38	4.88	4.97	6.65	7.64	5.03	4.43	4.83	5.92	4.50	5.32
Pr	1.18	0.80	0.72	0.70	0.74	1.03	1.09	0.78	0.69	0.77	0.87	0.73	0.77
Nd	6.04	4.16	3.96	3.53	3.92	5.46	5.53	4.13	3.53	3.91	4.58	3.38	3.68
Sm	1.96	1.39	1.47	1.19	1.28	1.75	1.75	1.40	1.17	1.34	1.49	1.22	1.34
Eu	0.70	0.53	0.44	0.43	0.43	0.68	0.79	0.44	0.49	0.51	0.56	0.49	0.47
Tb	0.53	0.34	0.34	0.31	0.33	0.47	0.45	0.37	0.32	0.35	0.40	0.31	0.34
Dy	3.29	2.21	2.27	2.12	2.12	2.88	2.90	2.30	2.08	2.18	2.41	2.25	2.19
Ho	0.72	0.47	0.47	0.44	0.43	0.64	0.61	0.52	0.45	0.48	0.49	0.46	0.47
Er	2.27	1.50	1.48	1.40	1.42	1.99	1.87	1.52	1.43	1.54	1.63	1.45	1.46
Tm	0.35	0.22	0.24	0.23	0.21	0.30	0.31	0.24	0.22	0.23	0.25	0.23	0.21
Yb	2.17	1.46	1.47	1.35	1.41	1.83	1.90	1.52	1.37	1.46	1.62	1.33	1.37
Lu	0.33	0.22	0.21	0.21	0.20	0.26	0.28	0.24	0.22	0.22	0.24	0.20	0.20
$\delta^{13}C_{PDB}$	nd	nd	nd	nd	nd	nd	−1.8	−1.4	nd	nd	nd	nd	nd

Table 1. (continued)

Basalt													
Type I													
96MB1045	96MB1047	96MB1049	96MB1050	96MB1051	96MB1052	96MB1054	96MB1058	96MB1062	96MB1063	96MB1064	96MB1065	96MB1066	96MB1073
62.47	65.22	63.55	62.20	62.34	63.68	59.84	62.18	58.15	62.28	55.92	61.39	50.23	52.15
1.03	1.05	1.04	1.05	1.11	1.04	1.20	1.03	1.04	1.04	0.98	1.02	1.10	1.09
14.9	15.4	15.1	14.6	15.1	14.8	16.2	14.4	14.3	14.4	14.8	14.6	15.9	15.5
13.50	11.51	12.54	14.25	13.63	12.70	14.84	13.93	13.67	12.94	13.34	13.31	12.65	12.11
0.050	0.035	0.066	0.062	0.075	0.049	0.094	0.068	0.162	0.092	0.184	0.066	0.167	0.159
5.82	3.65	5.72	6.25	5.64	5.45	6.05	5.54	5.82	6.01	5.70	6.32	6.06	4.98
0.13	0.14	0.12	0.15	0.15	0.13	0.13	0.75	4.76	0.97	6.46	1.45	11.47	11.69
		0.44	0.13		0.20		0.32	0.60	0.38	0.74	0.14	1.20	1.15
1.19	1.90	0.37	0.38	0.54	0.67	0.04	0.29	0.47	0.22	0.66	0.22	0.41	0.51
0.075	0.097	0.082	0.081	0.093	0.093	0.096	0.079	0.076	0.081	0.075	0.076	0.083	0.083
99.04	98.94	99.01	99.16	98.54	98.75	98.36	98.62	99.08	98.38	98.88	98.62	99.23	99.45
4.53	3.94	4.43	4.49	5.01	4.41	5.54	4.82	9.29	5.19	10.49	6.15	11.75	15.94
0.06	0.10	0.11	0.01	0.03	0.05	0.03	0.71	6.16	0.89	6.60	nd	7.83	8.86
40.9	34.3	44.6	46.6	44.7	34.3	55.6	35.6	35.2	39.0	45.1	37.6	54.9	40.0
361	314	455	430	394	302	586	373	340	345	444	329	411	362
244	191	327	286	312	213	289	236	183	209	197	210	229	208
48.1	41.2	53.5	60.5	62.2	45.6	70.8	49.7	53.7	52.4	74.0	56.3	87.7	59.7
88.2	90.0	190	155	211	87.5	204	162	141	151	222	192	200	141
102	105	42.7	81.5	162	12.3	184	157	130	155	81.9	54.5	233	148
242	139	128	159	146	194	228	185	184	252	211	158	97.8	
37.6	59.6	16.9	16.3	22.0	27.1	2.2	10.8	14.9	9.1	22.3	8.3	14.5	14.1
7.28	29.4	31.1	20.0	15.1	48.2	9.27	34.6	51.1	41.5	94.2	24.4	125	109
13.4	20.5	23.0	25.7	20.8	23.4	16.5	18.7	12.2	19.6	18.0	17.1	19.2	18.1
65.5	62.5	62.2	64.0	64.7	68.2	80.2	60.3	52.3	60.8	56.7	56.9	61.3	57.1
2.93	3.25	2.44	2.37	2.95	3.20	3.25	2.49	2.22	2.50	2.26	2.49	2.62	2.37
0.39	0.12		0.17	0.06	0.46	0.20	0.17	0.11	0.53			0.12	0.06
184	278	49	83	114	107	17	45	75	34	103	40	101	75
1.71	1.80	1.63	1.80	1.90	1.84	1.97	1.60	1.44	1.62	1.34	1.60	1.41	1.37
0.24	0.29	0.23	0.24	0.28	0.27	0.26	0.18	0.18	0.24	0.19	0.25	0.20	0.17
0.51	0.50	0.32	0.34	0.37	0.55	0.38	0.31	0.26	0.32	0.24	0.33	0.26	0.26
0.11	0.14	0.10	0.08	0.13	0.14	0.08	0.07	0.08	0.08	0.09	0.07	0.06	0.06
3.19	7.29	3.04	2.40	3.08	4.21	3.32	2.69	2.34	2.05	2.00	2.14	3.20	2.95
8.59	13.9	8.42	6.80	6.77	11.2	7.85	7.76	7.83	5.69	5.65	6.04	7.99	8.04
1.16	2.17	1.19	1.00	1.10	1.58	1.10	1.12	1.02	0.83	0.90	0.92	1.16	1.22
5.75	10.5	6.17	5.31	5.56	8.41	5.62	6.15	5.49	4.56	5.28	5.10	5.81	6.42
1.62	2.88	2.13	1.89	1.74	2.62	1.73	1.95	1.79	1.70	1.99	1.95	1.86	1.98
0.50	0.97	0.72	0.67	0.58	0.88	0.51	0.59	0.59	0.62	0.70	0.74	0.66	0.70
0.35	0.59	0.56	0.58	0.51	0.62	0.38	0.48	0.37	0.54	0.42	0.48	0.47	0.44
2.21	3.77	3.57	3.94	3.32	3.96	2.39	3.10	2.46	3.46	2.72	3.13	3.13	2.92
0.49	0.77	0.79	0.87	0.73	0.85	0.55	0.69	0.53	0.72	0.58	0.64	0.63	0.63
1.59	2.30	2.38	2.65	2.32	2.65	1.76	2.17	1.69	2.28	1.80	2.04	2.00	1.82
0.26	0.36	0.37	0.43	0.36	0.41	0.29	0.34	0.27	0.37	0.30	0.33	0.32	0.30
1.76	2.17	2.36	2.64	2.37	2.65	2.01	2.14	1.70	2.28	1.94	2.04	2.06	1.96
0.29	0.33	0.35	0.41	0.38	0.39	0.31	0.31	0.25	0.34	0.29	0.31	0.30	0.28
nd	nd	nd	nd	nd	nd	nd	nd	0.1	nd	1.4	nd	−0.5	−0.6

Table 1. (continued)

Lithology	Basalt												
Rock type	Type I												
Sample No.	96MB1075	96MB1076	96MB1078a	96MB1078b	96MB1079	96MB1084	96MB1085	96MB1086	96MB1087	96MB1089	96MB1091	96MB1092	96MB1095
SiO_2 (wt%)	65.37	61.33	51.91	63.31	63.22	51.19	51.75	49.95	50.01	52.16	52.72	53.21	51.53
TiO_2	0.99	1.02	0.99	1.01	1.03	1.09	1.09	1.13	1.02	1.09	1.10	1.10	1.06
Al_2O_3	14.7	13.9	14.5	15.0	14.8	15.2	14.9	16.2	15.1	15.1	15.1	15.2	14.9
Fe_2O_3t	12.27	15.73	14.28	13.59	13.00	14.39	13.58	15.77	13.58	13.78	13.95	13.91	13.79
MnO	0.066	0.064	0.290	0.037	0.043	0.231	0.183	0.122	0.174	0.188	0.185	0.161	0.294
MgO	4.88	5.35	5.53	5.11	5.86	5.77	7.31	9.99	7.02	7.19	7.12	6.68	6.29
CaO	0.14	0.67	9.61	0.12	0.12	9.89	9.75	5.53	11.60	7.55	7.00	6.96	8.88
Na_2O	0.65	0.16	0.33	0.39	0.26	0.69	0.48		0.39	1.90	1.84	1.35	0.43
K_2O	0.21	0.28	1.35	0.23	0.36	0.64	0.41	0.19	0.42	0.10	0.11	0.21	1.98
P_2O_5	0.087	0.074	0.075	0.065	0.062	0.079	0.081	0.086	0.074	0.080	0.082	0.082	0.081
Total	99.32	98.56	98.89	98.88	98.75	99.12	99.52	98.96	99.33	99.18	99.23	98.89	99.26
LOI	4.05	4.64	12.64	4.42	4.65	12.44	12.18	10.06	12.61	9.32	8.78	9.00	14.10
CO_2	0.03	0.64	9.22	0.05	0.03	8.40	7.11	4.28	8.22	4.90	4.39	4.06	10.82
Sc (ppm)	52.1	25.0	37.9	27.3	44.9	42.6	39.9	35.8	35.9	47.9	59.6	43.9	40.5
V	540	315	309	267	415	357	354	319	344	418	564	388	304
Cr	245	234	176	169	247	185	186	268	263	300	342	285	206
Co	54.5	72.0	73.7	53.9	67.1	64.1	57.2	77.0	66.0	67.5	88.0	63.1	38.3
Ni	189	186	168	158	222	145	181	173	166	189	204	147	116
Cu	121	121	164	75.9	212	225	109	102	110	229	145	182	168
Zn	221	228	163	134	251	284	136	96.1	122	110	171	115	102
Rb	7.2	8.8	38.7	7.0	13.1	19.0	14.9	9.3	17.0	6.6	8.2	9.3	47.4
Sr	55.9	34.3	67.5	34.7	44.9	77.7	65.2	34.2	50.8	47.7	67.1	51.4	90.0
Y	21.7	18.9	16.6	19.3	21.8	18.4	20.9	13.5	17.3	23.4	22.3	19.8	18.6
Zr	61.3	56.7	49.6	43.0	60.7	53.8	57.1	59.1	54.6	59.0	63.6	59.4	56.6
Nb	3.24	2.65	2.36	2.11	2.65	3.19	2.45	2.61	2.29	2.70	2.74	2.59	2.76
Mo	0.27	0.05	0.11	0.20	1.49	0.50	0.11		0.05		0.06	0.23	0.05
Ba	47	62	851	43	86	212	101	267	72	43	74	56	326
Hf	1.66	1.62	1.34	1.27	1.63	1.45	1.41	1.68	1.31	1.50	1.49	1.52	1.44
Ta	0.27	0.31	0.18	0.16	0.22	0.21	0.18	0.22	0.19	0.19	0.18	0.21	0.19
Th	0.34	0.31	0.25	0.21	0.28	0.27	0.29	0.31	0.27	0.29	0.27	0.29	0.31
U	0.07	0.07	0.06	0.05	0.12	0.09	0.08	0.08	0.06	0.07	0.06	0.06	0.36
La (ppm)	5.46	1.52	2.05	1.62	1.22	2.36	3.09	2.65	2.75	3.09	3.11	3.19	1.10
Ce	12.8	4.55	5.48	4.51	3.22	6.71	8.38	7.23	7.12	8.02	8.32	8.42	3.15
Pr	1.81	0.70	0.85	0.67	0.54	1.11	1.24	1.07	1.06	1.22	1.25	1.32	0.58
Nd	8.87	3.79	4.65	3.45	3.04	6.20	6.47	5.59	5.46	6.49	6.77	6.89	3.91
Sm	2.69	1.43	1.82	1.42	1.42	2.25	2.12	1.78	1.81	2.03	2.15	2.15	2.24
Eu	0.90	0.53	0.99	0.66	0.53	0.73	0.66	0.63	0.65	0.67	0.71	0.75	0.85
Tb	0.58	0.44	0.45	0.50	0.49	0.46	0.49	0.41	0.46	0.49	0.52	0.53	0.54
Dy	3.61	3.16	2.76	3.36	3.30	3.00	3.34	2.70	2.95	3.21	3.27	3.31	3.37
Ho	0.75	0.68	0.62	0.74	0.71	0.62	0.72	0.60	0.62	0.68	0.74	0.73	0.69
Er	2.30	2.12	1.84	2.23	2.23	2.01	2.19	1.83	1.95	2.10	2.17	2.21	2.22
Tm	0.36	0.34	0.29	0.35	0.35	0.30	0.35	0.29	0.30	0.35	0.36	0.37	0.36
Yb	2.25	2.08	1.96	2.16	2.22	2.08	2.13	1.96	1.86	2.13	2.18	2.14	2.10
Lu	0.33	0.30	0.28	0.32	0.34	0.33	0.34	0.31	0.29	0.33	0.34	0.33	0.31
$\delta^{13}C_{PDB}$	nd	nd	1.9	nd	nd	0.9	−0.4	−0.4	0.2	0.0	−0.2	0.1	−1.7

Table 1. (continued)

Basalt														
Type I				Type II										
96MB1096	96MB1097	96MB1100	96MB1108	96MB1043	96MB1044	96MB1056	96MB1057	96MB1059	96MB1067	96MB1077	96MB1080	96MB1081	96MB1082	
52.44	46.76	51.52	53.56	55.75	61.25	39.49	34.72	40.24	62.30	58.88	63.68	43.09	62.11	
1.05	0.94	0.96	1.02	0.63	0.85	0.98	0.69	0.85	1.04	1.07	0.81	0.78	0.90	
14.7	12.9	15.0	15.5	17.2	14.3	14.2	9.4	12.6	14.8	16.1	12.0	11.8	13.9	
12.47	16.26	12.60	13.35	12.55	12.64	8.89	24.89	8.65	12.35	18.48	16.06	15.80	15.29	
0.345	0.315	0.160	0.176	0.080	0.080	0.262	0.793	0.399	0.069	0.101	0.202	0.422	0.091	
5.84	8.17	7.56	6.91	12.00	9.08	4.48	8.07	6.94	3.63	1.16	4.26	9.36	5.33	
10.15	12.45	9.52	5.76	0.07	0.08	27.58	19.90	26.45	3.49	0.11	1.64	16.21	0.96	
0.65	0.31	1.05				0.70		0.44	0.46	1.53	0.15	0.46	0.10	
1.66	1.16	0.63	2.66	0.43		2.35	0.13	2.25	0.93	1.09	0.24	0.89	0.20	
0.081	0.074	0.077	0.073	0.041	0.045	0.078	0.050	0.063	0.093	0.088	0.065	0.075	0.078	
99.35	99.30	99.09	98.99	98.54	98.11	98.99	98.46	98.83	99.16	98.63	99.13	98.84	98.95	
13.57	16.82	13.91	10.83	6.80	5.83	22.70	20.53	23.52	5.99	4.58	6.81	19.86	5.92	
9.76	12.93	9.87	6.91	0.06	nd	nd	16.14	21.45	2.50	0.11	1.87	16.69	0.85	
45.7	31.9	45.0	49.6	26.4	30.1	29.8	21.7	27.4	42.5	44.6	28.5	27.7	32.4	
403	318	407	480	216	248	276	189	246	397	385	262	246	303	
264	196	229	162	193	238	133	112	154	251	285	255	168	218	
80.6	71.5	66.9	61.4	69.7	81.6	38.9	56.7	30.8	60.3	110	74.7	265	74.6	
218	178	146	133	402	407	52.8	87.7	84.4	128	352	619	1102	401	
12.7	78.3	39.7	271	113	200	79.3	81.8	42.8	111	156	68.5	185	106	
181	217	109	121	115	183	42.3	162	52.6	231	258	141	188	158	
69.9	31.1	18.8	85.0	13.8	2.0	52.1	3.8	52.0	31.6	35.7	7.8	21.5	7.8	
87.6	56.3	115	48.5	4.75	10.3	75.9	84.3	93.8	59.7	156	57.6	95.6	37.0	
21.5	17.3	17.3	17.9	8.97	11.0	13.1	12.5	11.5	18.4	11.8	13.0	9.28	16.9	
58.1	46.2	57.5	49.7	32.4	47.6	40.8	32.6	39.5	59.8	56.3	41.3	35.6	49.9	
2.27	1.99	2.08	2.13	1.43	2.14	2.03	1.82	6.86	2.72	2.59	1.95	1.53	2.27	
0.06			0.50	0.45	0.61	0.38	0.51	0.75	0.63	0.18	0.42	0.06	0.06	
350	284	126	286	72	77	845	42	621	239	348	182	240	48	
1.43	1.15	1.48	1.36	0.91	1.38	1.20	1.03	0.99	1.58	1.59	1.17	0.91	1.36	
0.18	0.17	0.17	0.36	0.15	0.20	0.23	0.21	0.81	0.20	0.23	0.15	0.11	0.18	
0.27	0.22	0.24	0.26	0.20	0.29	0.24	0.23	0.21	0.27	0.28	0.21	0.16	0.23	
0.41	0.39	0.35	0.51	0.05	0.05	0.36	0.31	0.40	0.08	0.07	0.07	0.17	0.06	
1.22	2.03	2.30	2.54	1.64	2.28	2.33	2.54	2.66	2.47	2.53	2.29	1.21	1.82	
3.52	5.31	6.31	6.74	4.18	6.26	5.44	6.05	6.54	7.33	6.59	7.08	2.93	5.19	
0.61	0.82	1.01	1.04	0.60	0.93	0.84	0.93	1.07	1.09	1.01	0.93	0.52	0.76	
3.92	4.35	5.66	5.60	2.99	4.68	4.27	4.59	5.17	5.66	5.27	4.73	3.09	4.00	
2.24	1.77	1.80	1.88	0.92	1.54	1.53	1.47	1.63	1.61	1.85	1.51	1.36	1.71	
0.92	0.72	0.67	0.65	0.32	0.43	0.84	0.76	0.70	0.62	0.61	0.62	0.54	0.60	
0.52	0.43	0.44	0.46	0.23	0.35	0.40	0.36	0.32	0.45	0.34	0.39	0.28	0.48	
3.33	2.75	2.71	2.94	1.43	2.10	2.53	2.22	2.02	3.03	2.03	2.40	1.71	3.12	
0.67	0.59	0.60	0.61	0.31	0.45	0.55	0.49	0.43	0.64	0.42	0.53	0.36	0.68	
2.13	1.80	1.87	1.83	0.97	1.47	1.67	1.55	1.34	1.95	1.29	1.65	1.09	2.17	
0.35	0.32	0.28	0.29	0.16	0.24	0.29	0.25	0.22	0.32	0.21	0.27	0.17	0.34	
2.07	1.81	1.85	1.89	1.07	1.54	1.68	1.60	1.44	1.93	1.35	1.66	1.11	2.22	
0.33	0.29	0.28	0.29	0.18	0.25	0.26	0.26	0.23	0.29	0.20	0.25	0.17	0.34	
0.0	0.5	0.1	−3.3	nd	nd	nd	0.1	0.7	0.6	nd	−2.0	−0.5	nd	

Table 1. (continued)

Lithology	Basalt												
Rock type	Type II												
Sample No.	96MB1083	96MB1088	96MB1090	96MB1099	96MB1101	96MB1102	96MB1104	96MB1105	96MB1106	96MB1107	96MB1109	96MB1111	96MB1113
SiO_2 (wt%)	55.62	51.34	53.62	46.93	41.12	30.77	38.64	59.00	46.03	49.34	38.21	44.93	30.70
TiO_2	0.98	1.09	1.10	0.97	0.99	0.77	1.00	1.00	0.92	1.08	0.87	0.79	0.71
Al_2O_3	13.6	15.1	15.3	15.4	15.5	10.8	15.5	15.6	14.3	15.2	14.2	12.0	10.6
Fe_2O_3t	21.00	13.61	11.43	9.47	10.46	7.20	16.91	13.74	12.03	13.65	8.62	8.16	7.57
MnO	0.261	0.160	0.177	0.323	0.207	0.160	0.273	0.072	0.197	0.205	0.281	0.208	0.174
MgO	5.82	7.96	5.06	1.95	4.44	9.54	5.87	7.64	8.18	6.80	0.80	2.09	6.98
CaO	0.38	9.35	9.38	20.64	22.83	37.38	19.43	0.19	15.67	10.83	23.05	28.78	40.15
Na_2O	0.02	0.25	3.42	0.03		0.53	0.43		0.89	1.24	0.10		0.10
K_2O	0.12	0.42	0.01	3.57	3.39	1.91	1.06	1.12	1.37	0.86	3.86	2.88	2.15
P_2O_5	0.077	0.084	0.084	0.090	0.101	0.062	0.067	0.075	0.073	0.074	0.061	0.073	0.038
Total	97.92	99.35	99.62	99.36	99.05	99.15	99.16	98.30	99.62	99.29	99.06	99.85	99.17
LOI	6.35	11.35	9.55	17.20	19.47	29.51	17.38	5.06	19.08	15.05	23.90	21.14	29.09
CO_2	0.25	6.29	6.36	13.48	14.25	27.99	12.78	0.15	16.11	11.46	21.22	18.50	26.89
Sc (ppm)	61.8	54.7	45.7	43.4	36.7	24.6	35.8	33.6	40.2	53.6	32.7	39.0	16.0
V	351	506	392	281	264	202	274	302	367	396	259	333	133
Cr	228	367	284	156	130	141	157	204	197	189	121	81.2	94.4
Co	80.8	78.3	59.2	49.8	48.4	18.2	56.7	50.1	56.5	71.6	36.1	33.1	18.3
Ni	196	196	139	101	120	43.4	147	145	157	108	88.2	62.0	60.4
Cu	151	72.5	127	35.4	55.0	44.7	15.7	20.0	196	11.0	64.7	70.8	13.9
Zn	255	146	104	63.9	128	37.8	134	135	131	140	40.9	49.8	44.1
Rb	6.0	19.2	3.1	88.6	76.7	40.4	24.2	31.3	46.6	30.5	72.7	84.9	41.0
Sr	36.2	51.6	52.7	48.3	38.1	136	65.1	3.32	140	123	160	28.9	61.5
Y	18.9	21.1	20.2	30.6	9.19	10.8	12.9	21.5	13.8	19.2	12.5	19.3	8.33
Zr	52.9	60.1	57.0	51.7	45.2	33.0	42.4	53.4	42.5	51.6	40.0	41.7	23.3
Nb	6.10	3.36	2.58	2.55	1.80	1.29	2.49	2.31	2.05	2.09	1.79	2.02	1.14
Mo	0.66	0.13	0.10	0.71	0.44	0.33	0.14		0.11	0.17	0.33	0.07	0.23
Ba	67	306	10	118	191	310	101	156	239	188	396	587	372
Hf	1.53	1.45	1.48	1.16	1.16	0.85	1.22	1.48	1.07	1.36	1.08	1.00	0.66
Ta	0.22	0.24	0.19	0.24	0.23	0.10	0.22	0.22	0.15	0.31	0.19	0.12	0.10
Th	0.26	0.31	0.28	0.28	0.26	0.18	0.24	0.30	0.20	0.24	0.21	0.19	0.14
U	0.09	0.08	0.06	0.15	0.19	0.32	0.07	0.06	0.51	0.12	0.36	0.19	0.14
La (ppm)	2.57	3.60	3.09	3.65	2.35	2.32	1.77	1.77	1.53	2.30	2.46	1.94	1.91
Ce	7.14	12.4	8.06	10.0	6.22	5.61	4.64	4.17	3.99	6.32	7.09	4.61	4.38
Pr	1.08	1.26	1.19	1.59	0.97	0.90	0.75	0.65	0.63	1.00	0.88	0.73	0.75
Nd	5.78	6.28	6.42	8.82	5.07	4.45	4.18	3.43	3.49	5.70	4.32	3.72	3.71
Sm	2.04	2.11	1.94	3.00	1.49	1.12	1.62	1.31	1.38	1.83	1.48	1.40	1.14
Eu	0.68	0.72	0.57	0.99	0.51	0.51	0.69	0.61	0.52	0.74	0.65	0.77	0.60
Tb	0.53	0.50	0.50	0.69	0.28	0.27	0.44	0.51	0.35	0.47	0.32	0.44	0.26
Dy	3.50	3.21	3.12	4.57	1.73	1.66	2.86	3.47	2.21	3.18	2.03	2.89	1.56
Ho	0.76	0.68	0.67	0.99	0.37	0.38	0.61	0.78	0.45	0.70	0.45	0.61	0.32
Er	2.34	2.11	2.07	3.13	1.20	1.11	1.90	2.38	1.42	2.04	1.33	2.00	1.00
Tm	0.35	0.34	0.34	0.50	0.21	0.19	0.34	0.37	0.22	0.31	0.23	0.32	0.17
Yb	2.31	2.05	2.02	3.08	1.31	1.10	1.96	2.22	1.43	2.08	1.40	1.88	1.07
Lu	0.35	0.32	0.31	0.48	0.21	0.18	0.30	0.34	0.21	0.30	0.20	0.29	0.15
$\delta^{13}C_{PDB}$	nd	−0.5	0.5	−1.1	1.8	−0.2	0.7	nd	−0.5	0.8	−0.1	−2.4	−3.4

Table 1. (continued)

Basalt													
Type II													
96MB1114	96MB1115	96MB1116	96MB1117	96MB1118	96MB1119	96MB1120	96MB1128	96MB1129	96MB1133	96MB1136	96MB1140	96MB1144	96MB1145
34.30	54.26	62.01	54.02	65.69	64.38	53.76	42.43	43.83	60.11	63.07	55.46	55.51	61.80
0.81	1.59	1.68	2.76	1.65	0.94	2.60	0.45	0.57	0.68	0.61	0.71	0.73	0.72
11.2	13.2	11.8	13.1	11.8	12.9	12.9	10.8	12.4	16.7	16.7	16.2	14.3	14.3
9.88	16.65	18.33	20.81	15.42	14.35	23.16	7.81	8.73	10.37	10.43	15.90	15.10	11.82
0.220	0.171	0.050	0.224	0.088	0.041	0.083	0.146	0.188	0.074	0.036	0.080	0.104	0.064
8.20	7.47	4.16	6.30	1.17	5.97	5.49	14.09	16.03	9.26	6.59	9.91	13.23	9.47
31.34	4.43	0.13	0.14	0.38	0.12	0.13	22.32	15.91	0.11	0.07	0.12	0.11	0.18
2.95	1.22	0.57	0.63	2.74	0.86	0.19	1.31	1.63	2.10	1.81	0.47		0.87
0.053	0.105	0.084	0.115	0.239	0.064	0.092	0.034	0.049	0.046	0.031	0.049	0.054	0.052
98.93	98.97	98.63	97.98	99.09	99.52	98.22	99.26	99.17	99.28	99.26	98.74	99.00	99.16
26.53	9.23	3.79	5.17	3.18	4.14	5.07	22.67	20.48	5.26	4.65	6.02	6.46	5.31
24.07	5.06	0.03	0.07	0.07	0.06	0.04	19.96	17.28	0.07	0.03	0.11	0.03	0.05
23.6	42.8	46.9	62.7	32.7	55.5	57.3	23.4	38.3	41.6	31.4	26.1	26.1	19.5
177	440	902	1121	75.2	447	1357	147	229	225	237	198	229	304
92.4	7.93	4.10	3.16	0.97	57.4	1.67	220	246	310	435	153	216	239
25.1	52.3	64.1	97.0	19.2	77.6	87.7	29.4	55.6	35.3	35.8	51.9	76.2	96.5
48.6	35.9	51.6	60.0	10.6	104	18.5	89.3	117	119	139	290	536	801
6.44	3.08	203	7.16	1.80	195	32.1	86.0	163	121	77.2	13.7	13.8	53.0
33.1	125	174	206	104	200	188	52.8	74.7	83.3	82.8	135	161	143
51.0	33.4	20.7	18.8	68.6	30.1	8.0	31.6	46.1	59.3	48.9	13.1	1.0	35.2
44.8	34.3	8.43	15.2	11.1	3.47	9.14	224	259	2.91	6.16	5.57	2.65	11.5
9.81	25.3	21.1	64.1	31.7	18.6	22.4	7.30	6.11	11.1	13.5	6.81	15.0	15.8
31.0	71.1	67.6	92.1	180	50.9	77.7	16.2	24.5	31.2	24.5	34.4	36.4	39.0
1.81	3.26	2.71	4.36	6.52	2.24	3.36	1.24	1.03	1.20	1.54	1.70	1.88	2.72
0.63	0.05	0.10	0.05	0.09	0.11	0.21	0.21	0.05		0.31	0.26	0.66	0.14
601	231	100	359	343	184	63	339	654	200	148	126	14	274
0.90	2.09	1.94	2.55	5.29	1.40	2.25	0.50	0.61	0.89	0.66	1.00	0.98	0.97
0.10	0.39	0.29	0.37	0.67	2.16	0.39	0.10	0.08	0.12	0.10	0.14	0.14	0.14
0.18	0.39	0.36	0.50	0.95	0.25	0.40	0.10	0.11	0.16	0.13	0.23	0.22	0.20
0.19	0.11	0.10	0.10	0.23	0.07	0.10	0.13	0.10	0.05	0.04	0.05	0.07	0.07
1.10	4.24	3.45	10.2	6.46	3.10	3.24	1.24	1.43	2.54	2.97	2.37	2.29	2.43
2.58	11.2	9.53	24.5	19.4	8.02	7.87	4.30	2.96	5.83	6.87	3.39	5.41	5.37
0.45	1.70	1.40	3.59	2.96	1.20	1.13	0.56	0.52	0.96	1.01	0.60	0.79	0.83
2.73	9.23	7.43	19.1	15.7	6.26	6.05	2.64	2.67	4.65	5.05	2.96	3.99	4.33
1.42	2.98	2.21	6.01	4.75	1.87	2.11	0.88	0.85	1.38	1.55	0.91	1.27	1.38
0.60	0.98	0.66	1.97	1.26	0.65	0.87	0.34	0.45	0.37	0.57	0.29	0.45	0.53
0.33	0.70	0.55	1.60	1.02	0.48	0.61	0.22	0.19	0.34	0.34	0.23	0.38	0.34
2.24	4.42	3.50	10.1	6.36	3.14	4.01	1.44	1.13	2.13	2.24	1.42	2.72	2.42
0.44	0.94	0.77	2.17	1.43	0.70	0.87	0.28	0.24	0.47	0.47	0.30	0.61	0.50
1.40	2.83	2.41	6.34	4.42	2.08	2.64	0.87	0.75	1.43	1.42	0.93	1.86	1.63
0.20	0.44	0.36	0.95	0.71	0.32	0.41	0.15	0.12	0.21	0.22	0.16	0.32	0.23
1.51	2.76	2.37	5.49	4.16	2.03	2.64	0.87	0.87	1.43	1.27	1.01	1.89	1.51
0.21	0.41	0.33	0.81	0.64	0.28	0.40	0.14	0.13	0.19	0.18	0.15	0.28	0.23
−0.6	−1.8	nd	nd	nd	nd	nd	1.2	−0.9	nd	nd	nd	nd	nd

Table 1. (continued)

Lithology	Basalt											
Rock type	Type II		Highly silicified					Interpillow material				
Sample No.	96MB1147	96MB1148	96MB1048	96MB1053	96MB1055	96MB1074	96MB1098	96MB1060	96MB1061	96MB1068	96MB1093	96MB1094
SiO_2 (wt%)	65.45	57.74	84.34	83.06	91.14	80.04	76.39	18.00	35.68	21.26	38.67	50.80
TiO_2	0.97	1.25	0.63	0.71	0.25	1.02	0.95		0.22	0.74	0.72	0.41
Al_2O_3	14.3	16.9	10.0	11.6	6.2	14.3	16.1	0.1	3.1	9.7	9.9	7.9
Fe_2O_3t	11.99	14.14	1.63	0.72	0.26	0.67	1.08	17.18	33.21	13.32	14.26	11.48
MnO	0.061	0.056	0.006	0.005	0.009	0.005	0.027	1.282	1.176	0.693	0.606	0.540
MgO	4.64	8.46	0.37	0.26	0.08	0.07	0.18	16.49	4.24	4.31	4.72	4.37
CaO	0.15	0.13	0.06	0.06	0.12	0.16	0.50	45.66	20.39	48.16	31.14	24.73
Na_2O					0.04	0.98	0.07			0.03		
K_2O	1.60	0.25	2.60	3.39	1.41	2.12	4.50		0.21	0.14	0.03	
P_2O_5	0.091	0.046	0.043	0.025	0.010	0.077	0.014	0.009	0.065	0.065	0.020	0.057
Total	99.15	98.92	99.54	99.77	99.52	99.47	99.82	98.53	98.16	98.38	99.84	100.10
LOI	3.93	5.91	1.61	1.50	1.08	2.16	2.39	36.45	19.60	29.54	21.84	18.59
CO_2	0.03	0.01	nd	0.03	0.08	0.03	nd	36.62	nd	nd	19.61	16.65
Sc (ppm)	37.6	69.7	26.3	22.8	10.0	19.0	65.1	1.58	13.5	26.9	24.2	17.6
V	322	554	250	244	114	308	672	32.1	113	199	174	207
Cr	290	395	196	114	231	129	224		37.5	122	127	88.0
Co	38.8	54.8	9.86	3.25	2.61	8.38	31.1	6.25	67.8	51.8	45.4	60.4
Ni	86.2	149	75.1	38.9	17.3	45.3	48.0	31.7	153	104	84.6	112
Cu	68.9	93.2	49.6	44.1	14.2	57.8	107		219	136	129	742
Zn	158	268	32.3	20.2	18.1	55.9	18.2	25.8	126	97.1	138	106
Rb	42.6	8.1	88.6	95.8	40.8	61.7	140	0.8	7.5	2.3	3.0	2.6
Sr	9.72	24.9	18.8	11.0	13.2	76.1	11.3	83.1	27.2	71.0	125	78.7
Y	17.4	17.4	9.36	15.7	8.65	13.9	5.76	21.3	13.7	16.5	20.1	26.1
Zr	58.1	79.7	41.1	38.2	13.9	62.0	55.1	2.06	10.8	23.1	21.3	20.8
Nb	2.75	3.51	1.92	2.16	0.44	2.50	3.38	0.28	0.75	1.67	1.56	1.34
Mo	0.34	0.33	0.22	0.61	0.15		0.88	0.16	2.83	0.62	0.51	0.56
Ba	113	116	211	208	186	489	261	7	74	35	105	4
Hf	1.53	1.90	0.98	1.07	0.38	1.51	1.28	0.04	0.31	0.85	0.82	0.54
Ta	0.21	0.28	0.16	0.18	0.03	0.22	0.21	0.05	0.04	0.10	0.22	0.07
Th	0.42	0.60	0.22	0.25	0.05	0.28	0.31		0.06	0.15	0.15	0.10
U	0.10	0.14	0.18	0.10	0.04	0.16	0.30	0.11	0.31	0.05	0.04	0.03
La (ppm)	3.21	5.22	6.61	2.71	1.02	3.30	8.61	0.91	1.44	2.28	3.86	2.62
Ce	8.28	10.7	10.4	7.68	2.80	14.6	24.8	1.79	3.12	5.21	8.76	6.17
Pr	1.19	1.65	1.71	1.04	0.46	1.25	3.29	0.37	0.49	0.80	1.39	0.97
Nd	5.70	8.16	7.50	5.16	2.72	5.85	15.6	1.57	2.88	4.17	7.43	5.41
Sm	1.64	2.40	1.93	1.64	1.02	1.58	3.46	0.93	1.40	1.43	2.58	2.02
Eu	0.50	0.74	0.60	0.57	0.46	0.60	1.00	0.76	0.84	0.60	1.31	0.72
Tb	0.37	0.45	0.30	0.38	0.24	0.41	0.32	0.31	0.33	0.47	0.58	0.54
Dy	2.42	2.78	1.62	2.39	1.42	2.66	1.28	2.34	2.09	2.86	3.55	3.35
Ho	0.51	0.58	0.33	0.53	0.31	0.49	0.21	0.53	0.44	0.62	0.70	0.71
Er	1.68	1.80	0.96	1.63	0.92	1.31	0.56	1.76	1.37	1.93	2.00	2.12
Tm	0.27	0.29	0.16	0.25	0.14	0.18	0.09	0.26	0.21	0.30	0.32	0.33
Yb	1.73	1.87	1.02	1.57	0.91	0.97	0.52	1.33	1.19	1.74	1.96	2.04
Lu	0.25	0.30	0.15	0.24	0.12	0.12	0.07	0.22	0.20	0.25	0.30	0.33
$\delta^{13}C_{PDB}$	nd	nd	nd	nd	nd	nd	nd	−2.0	nd	nd	0.9	0.9

Fe_2O_3t = total iron as Fe_2O_3; nd = not determined.
No entry indicates data below detection limit.

Table 2. Averages, maxima, minima, and standard deviations (σ) of each lithology.

Lithology	Dolerite								Basalt			
Rock type	The least altered (N = 5)				Altered (N = 8)				Type I (N = 31)			
	Avg	Max	Min	Stdev	Avg	Max	Min	Stdev	Avg	Max	Min	Stdev
SiO_2 (wt%)	49.13	51.27	47.40	1.47	49.76	52.29	47.93	1.25	56.89	65.37	46.76	5.78
TiO_2	0.72	0.98	0.61	0.15	0.69	0.87	0.58	0.10	1.05	1.20	0.94	0.05
Al_2O_3	15.6	17.1	14.0	1.1	16.2	17.1	14.8	0.6	14.9	16.2	12.9	0.6
Fe_2O_3t	12.05	13.32	10.60	1.00	11.50	13.77	10.10	1.14	13.59	16.26	11.51	1.07
MnO	0.175	0.192	0.157	0.013	0.170	0.202	0.154	0.016	0.141	0.345	0.035	0.088
MgO	9.30	12.33	7.04	2.48	8.11	9.24	7.26	0.55	6.18	9.99	3.65	1.14
CaO	10.69	12.31	9.22	1.41	10.45	13.07	7.04	2.19	4.97	12.45	0.12	4.60
Na_2O	1.85	2.34	1.61	0.30	2.30	2.91	1.58	0.52	0.52	1.90		0.52
K_2O	0.17	0.26	0.10	0.08	0.33	1.01	0.04	0.38	0.66	2.66	0.04	0.64
P_2O_5	0.051	0.067	0.044	0.009	0.047	0.057	0.039	0.006	0.080	0.097	0.062	0.008
LOI	3.57	4.44	2.67	0.77	4.04	7.93	2.75	1.91	8.71	16.82	3.94	4.08
CO_2	0.38	0.92	0.09	0.47	0.84	3.82	0.03	1.42	4.43	12.93	0.01	4.19
Sc (ppm)	35.0	42.0	29.7	4.50	44.9	77.6	31.6	14.0	41.7	59.6	25.0	7.92
V	261	305	224	32.5	301	582	224	116	385	586	267	78.0
Cr	257	493	12.9	197	432	691	101	215	235	342	162	48.4
Co	70.8	113	48.4	26.6	62.0	104	41.8	18.2	62.5	88.0	38.3	12.4
Ni	280	571	67.7	207	142	186	76.3	36.5	166	222	87.5	37.7
Cu	144	173	104	30.9	162	200	112	32.3	129	271	12.3	65.7
Zn	90.2	131	74.1	23.5	87.1	140	68.1	24.9	171	284	96.1	52.8
Rb	5.5	8.4	3.0	2.7	10.0	27.3	2.0	10.7	22.2	85.0	2.2	19.7
Sr	129	188	90.5	40.1	138	201	54.1	43.2	53.9	125	7.28	30.4
Y	13.5	17.7	11.6	2.47	14.3	21.9	12.0	3.17	19.1	25.7	12.2	3.04
Zr	35.7	46.2	29.8	6.68	35.5	49.3	29.8	6.15	58.7	80.2	43.0	6.86
Nb	1.61	2.25	1.28	0.39	1.54	2.13	1.22	0.30	2.59	3.25	1.99	0.37
Mo	0.26	0.52	0.06	0.18	0.13	0.22	0.06	0.05	0.19	1.49		0.30
Ba	47	69	24	16	106	315	30	110	148	851	17	162
Hf	1.01	1.39	0.76	0.23	0.94	1.18	0.77	0.14	1.54	1.97	1.15	0.20
Ta	0.14	0.20	0.11	0.03	0.20	0.86	0.09	0.26	0.22	0.36	0.16	0.05
Th	0.20	0.28	0.16	0.05	0.19	0.24	0.16	0.03	0.31	0.55	0.21	0.08
U	0.05	0.06	0.05	0.00	0.05	0.07	0.03	0.01	0.13	0.51	0.05	0.12
La (ppm)	2.13	2.90	1.88	0.43	2.13	2.97	1.70	0.45	2.75	7.29	1.10	1.22
Ce	5.55	7.40	4.88	1.05	5.54	7.64	4.43	1.13	7.17	13.9	3.15	2.43
Pr	0.83	1.18	0.70	0.20	0.84	1.09	0.69	0.14	1.08	2.17	0.54	0.34
Nd	4.32	6.04	3.53	0.98	4.28	5.53	3.38	0.84	5.72	10.5	3.04	1.56
Sm	1.46	1.96	1.19	0.30	1.43	1.75	1.17	0.22	1.96	2.88	1.42	0.34
Eu	0.50	0.70	0.43	0.11	0.55	0.79	0.44	0.12	0.70	0.99	0.50	0.13
Tb	0.37	0.53	0.31	0.09	0.38	0.47	0.31	0.06	0.48	0.62	0.35	0.07
Dy	2.40	3.29	2.12	0.50	2.40	2.90	2.08	0.32	3.13	3.96	2.21	0.42
Ho	0.51	0.72	0.43	0.12	0.52	0.64	0.45	0.07	0.67	0.87	0.49	0.09
Er	1.61	2.27	1.40	0.37	1.61	1.99	1.43	0.21	2.08	2.65	1.59	0.26
Tm	0.25	0.35	0.21	0.06	0.25	0.31	0.21	0.04	0.33	0.43	0.26	0.04
Yb	1.57	2.17	1.35	0.34	1.55	1.90	1.33	0.22	2.10	2.65	1.70	0.22
Lu	0.23	0.33	0.20	0.06	0.23	0.28	0.20	0.03	0.32	0.41	0.25	0.03
$\delta^{13}C_{PDB}$	nd	nd	nd	nd	−1.6	−1.4	−1.8	0.2	−0.1	1.9	−3.3	1.1

Table 2. (continued)

Basalt											
Type II (N = 39)				Highly silicified (N = 5)				Interpillow material (N = 5)			
Avg	Max	Min	Stdev	Avg	Max	Min	Stdev	Avg	Max	Min	Stdev
51.32	65.69	30.70	10.47	83.00	91.14	76.39	5.49	32.88	50.80	18.00	13.41
1.01	2.76	0.45	0.48	0.71	1.02	0.25	0.31	0.52	0.74		0.25
13.8	17.2	9.4	2.0	11.7	16.1	6.2	3.9	6.1	9.9	0.1	4.3
13.44	24.89	7.20	4.38	0.87	1.63	0.26	0.52	17.89	33.21	11.48	8.81
0.176	0.793	0.036	0.140	0.010	0.027	0.005	0.009	0.859	1.282	0.540	0.344
6.87	16.03	0.80	3.45	0.19	0.37	0.07	0.12	6.82	16.49	4.24	5.40
10.52	40.15	0.07	12.36	0.18	0.50	0.06	0.18	34.02	48.16	20.39	12.41
0.28	3.42		0.63	0.22	0.98		0.43	0.01	0.03		0.01
1.29	3.86		1.08	2.80	4.50	1.41	1.19	0.08	0.21		0.09
0.073	0.239	0.031	0.034	0.034	0.077	0.010	0.027	0.043	0.065		0.027
12.42	29.51	3.18	8.42	1.75	2.39	1.08	0.53	25.20	36.45	18.59	7.61
8.17	27.99	0.01	9.37	0.05	0.08	0.03	0.03	24.29	36.62	16.65	10.78
37.5	69.7	16.0	12.9	28.6	65.1	9.98	21.3	16.7	26.9	1.58	10.0
354	1357	75.2	253	317	672	114	210	145	207	32.1	73.0
180	435	0.97	108	179	231	114	54.2	74.8	127		55.0
62.0	265	18.2	40.5	11.0	31.1	2.61	11.6	46.3	67.8	6.25	23.9
201	1102	10.6	229	44.9	75.1	17.3	20.7	97.2	153	31.7	44.3
81.0	203	1.80	62.6	54.5	107	14.2	33.6	245	742		288
132	268	33.1	65.0	28.9	55.9	18.1	16.2	98.6	138	25.8	43.7
33.6	88.6	1.0	23.9	85.4	140	40.8	37.7	3.2	7.5	0.8	2.5
58.8	259	2.65	62.6	26.1	76.1	11.0	28.2	77.0	125	27.2	34.8
16.6	64.1	6.11	9.87	10.7	15.7	5.76	4.04	19.5	26.1	13.7	4.77
49.9	180	16.2	26.9	42.0	62.0	13.9	18.5	15.6	23.1	2.06	8.98
2.52	6.86	1.03	1.37	2.08	3.38	0.44	1.07	1.12	1.67	0.28	0.59
0.28	0.75		0.23	0.37	0.88		0.36	0.94	2.83	0.16	1.07
247	845	10	196	271	489	186	125	45	105	4	44
1.36	5.29	0.50	0.79	1.04	1.51	0.38	0.43	0.51	0.85	0.04	0.34
0.27	2.16	0.08	0.34	0.16	0.22	0.03	0.08	0.09	0.22	0.04	0.07
0.27	0.95	0.10	0.15	0.22	0.31	0.05	0.10	0.09	0.15		0.07
0.14	0.51	0.04	0.11	0.16	0.30	0.04	0.10	0.11	0.31	0.03	0.12
2.78	10.2	1.10	1.61	4.45	8.61	1.02	3.08	2.22	3.86	0.91	1.14
7.14	24.5	2.58	4.20	12.0	24.8	2.80	8.32	5.01	8.76	1.79	2.71
1.07	3.59	0.45	0.61	1.55	3.29	0.46	1.07	0.80	1.39	0.37	0.41
5.55	19.1	2.64	3.24	7.37	15.6	2.72	4.92	4.29	7.43	1.57	2.26
1.81	6.01	0.85	0.98	1.93	3.46	1.02	0.92	1.67	2.58	0.93	0.64
0.66	1.97	0.29	0.29	0.65	1.00	0.46	0.21	0.85	1.31	0.60	0.27
0.44	1.60	0.19	0.25	0.33	0.41	0.24	0.07	0.44	0.58	0.31	0.12
2.85	10.1	1.13	1.57	1.87	2.66	1.28	0.61	2.84	3.55	2.09	0.63
0.61	2.17	0.24	0.34	0.37	0.53	0.21	0.13	0.60	0.71	0.44	0.11
1.89	6.34	0.75	1.01	1.08	1.63	0.56	0.41	1.84	2.12	1.37	0.29
0.30	0.95	0.12	0.15	0.16	0.25	0.09	0.06	0.28	0.33	0.21	0.05
1.87	5.49	0.87	0.88	1.00	1.57	0.52	0.37	1.65	2.04	1.19	0.38
0.28	0.81	0.13	0.13	0.14	0.24	0.07	0.06	0.26	0.33	0.20	0.05
−0.4	1.8	−3.4	1.3	nd	nd	nd	nd	0.0	1.7	0.9	−2.0

Fe_2O_3t = total iron as Fe_2O_3; nd = not determined.
No entry indicates data below detection limit.

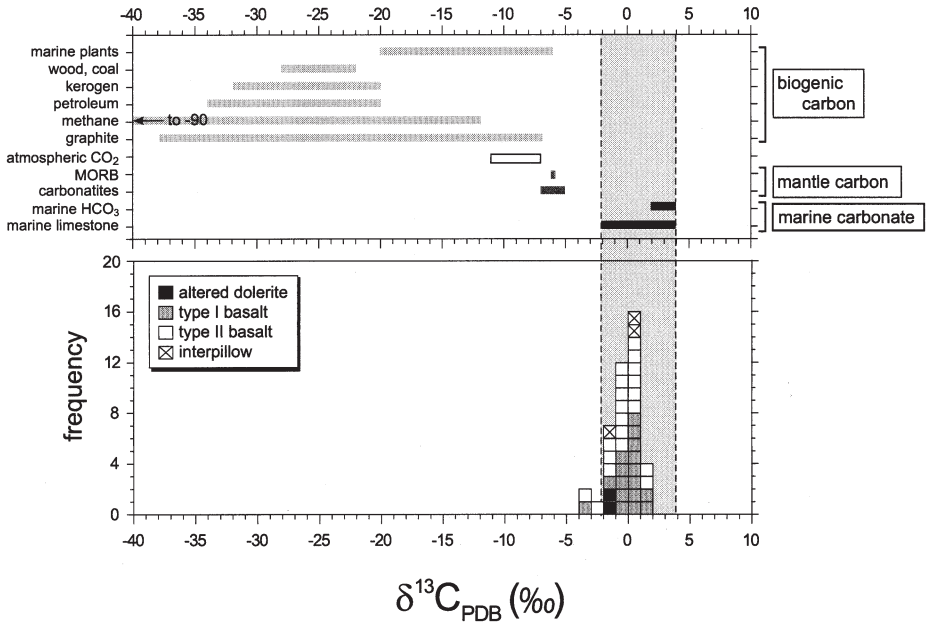

Fig. 6. Histogram of C isotope ratios of basalt and dolerite. Typical ranges of the $\delta^{13}C$ values of marine carbonates, mantle carbons, and biogenic carbons are from Criss (1995).

contents of dolerite and basalt are significantly high. The Sr content of dolerite is slightly high, and that of type I and type II is high in some samples and low in other samples. These elements are well known as highly mobile elements, and hence the enrichment and depletion of these elements (Rb, Ba, K, Sr) are probably caused by hydrothermal alteration. The type I and type II basalts have generally higher average contents of TiO_2, V, and Zr, and lower Ni and Cr contents than the dolerite. However, it is uncertain that these geochemical signatures are caused by a primary igneous

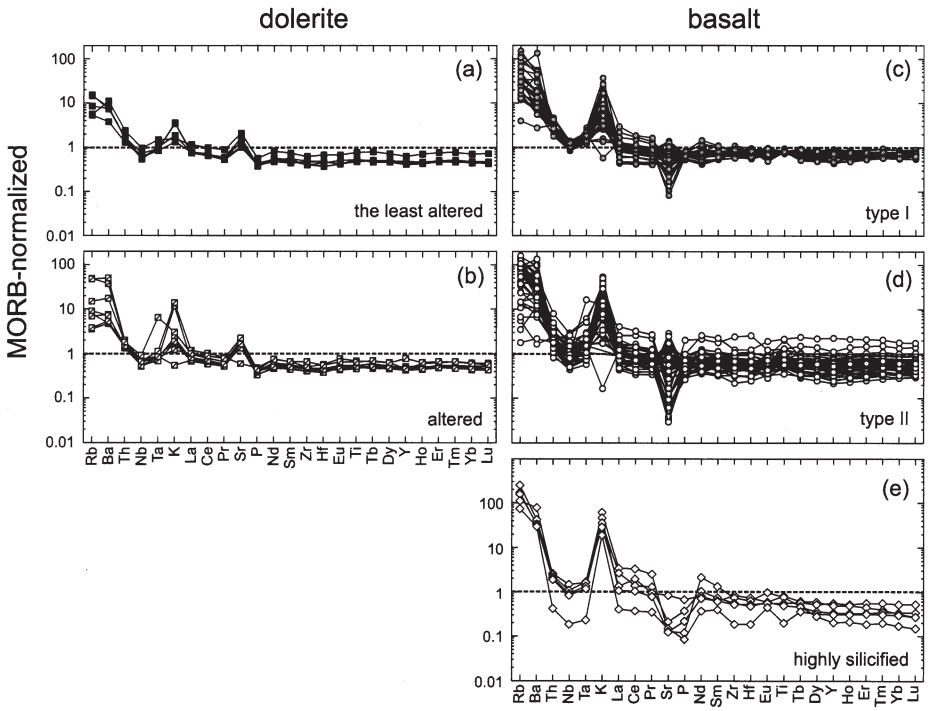

Fig. 7. MORB-normalized spider diagrams for (a) the least altered dolerite, (b) altered dolerite, (c) type I basalt, (d) type II basalt, and (e) highly silicified basalt. Normalizing MORB values are after Sun and McDonough (1989).

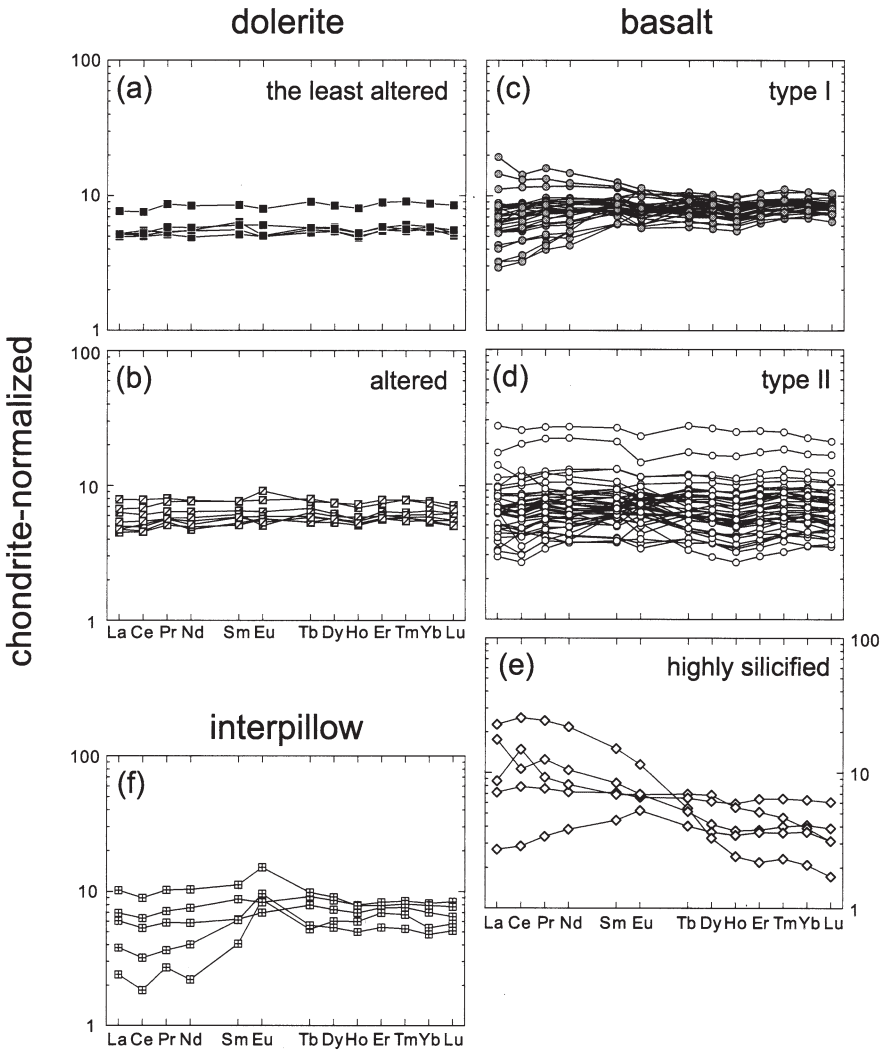

Fig. 8. Chondrite-normalized REE patterns for (a) the least altered dolerite, (b) altered dolerite, (c) type I basalt, (d) type II basalt, (e) highly silicified basalt, and (f) interpillow material. Normalizing chondrite values are after Masuda et al. (1973) and Masuda (1975).

variation (from more primitive dolerite to more evolved basalt), as the compositional range of these elements in the dolerite is within the wide range of basalt (Table 2).

Chondrite-normalized REE patterns are shown in Figure 8. The REE patterns of dolerite and basalt mostly show flat or slightly light REE (LREE)-depleted patterns (Fig. 8a, b, c, d), although three samples of type I basalt are slightly enriched in LREE (Fig. 8c). Their elemental abundances are generally one order of magnitude higher than chondritic abundances. These features on the REE pattern are also similar to those of modern MORB (e.g., Hofmann, 1988). Highly silicified basalts exhibit LREE-enriched patterns for three samples and generally flat patterns for two samples (Fig. 8e). Interpillow materials show relatively flat patterns for three samples and slightly LREE-depleted patterns for two samples (Fig. 8f). Significantly positive Eu anomalies are observable in some parts of type I, type II and interpillow samples (Fig. 8c, d, f).

6. DISCUSSION

6.1. Origin of Carbonate Carbon

The $\delta^{13}C$ values of carbonate carbons in the altered basaltic rocks are mostly 0 ± 2 ‰. The range of the $\delta^{13}C$ values is relatively narrow and almost the same as those of marine carbonates and limestones (Fig. 6), indicating that the carbonate carbon in the altered samples is derived from seawater and that contamination by mantle and biogenic carbon is negligible. This isotopic result is consistent with our geological interpretation that the basaltic rocks were subject to the seafloor hydrothermal carbonatization and were not subject to the fault-related carbonatization. The narrow $\delta^{13}C$ values close to zero also imply a quite minor influence of regional (superimposed) metamorphism and modern weathering. Metamorphic reworking of the seafloor hydrothermal carbonates greatly and variably shifts the $\delta^{13}C$ values toward negative values through isotope fractionation (Bottinga, 1969). Diagenetic and weath-

ered carbonates are also characterized by a considerably wide range of $\delta^{13}C$ and relatively low $\delta^{13}C$ values, reflecting various degrees of contributions from dissolved CO_2 derived from the decay of organic matter (e.g., Heydari et al., 2001; Knauth et al., 2003; Krishnamurthy et al., 2003). Therefore, the alteration of $\delta^{13}C$ values due to superimposed metamorphism and weathering seems negligible in our samples.

6.2. Alteration Reaction

The alteration mineral assemblage of type I and type II basalts is characterized by the presence of carbonate and K-mica and the absence of Ca-Al silicate minerals such as epidote and actinolite, whereas that of dolerite is typical greenschist assemblage of chlorite + epidote + albite + quartz ± actinolite. Some thermodynamic studies pointed out that this type of mineral assemblage (carbonate and aluminosilicates such as K-mica and chlorite instead of Ca-Al silicates) occurs in the high-μCO_2 condition (e.g., Zen, 1961; Thompson, 1971; Seki, 1973; Kishida and Kerrich, 1987; Miyashiro, 1994). This suggests that the carbonatized basalt was altered by a hydrothermal fluid with a high-CO_2 concentration.

In our samples, plagioclase in the basalt is replaced by K-mica, carbonate, and quartz, whereas plagioclase in the dolerite is replaced by epidote and albite. Mafic minerals/glass in the basalt are replaced by chlorite, carbonate, and quartz, whereas those in the dolerite are replaced by chlorite, actinolite, and epidote. These differences of alteration mineral assemblages between basalt and dolerite can be explained by the following reactions:

Plagioclase:

$$3\text{albite} + 2\text{epidote} + 4CO_2 + 2H_2O + 3K^+ = 3\text{K-mica} + 4\text{calcite} + 6\text{quartz} + 3Na^+ \quad (1)$$

Mafic minerals/glass:

$$2\text{epidote} + 3\text{actinolite} + 10CO_2 + 8H_2O = 3\text{chlorite} + 10\text{calcite} + 21\text{quartz} \quad (2)$$

$$\text{actinolite} + 3\text{calcite} + 7CO_2 = 5\text{ankerite} + 8\text{quartz} + H_2O \quad (3)$$

Because the dolerite occurs within the basalt unit, these differences between basalt and dolerite are probably caused by the difference in water/rock ratio depending on their porosity. It is likely that higher water/rock ratio in the basalt (mostly pillowed basalt) than in the massive dolerite led to supply sufficient CO_2 from the fluid to basalt.

The alteration mineral assemblage of the dolerite in the pillow basalt unit suggests that the alteration temperature of the upper part of the Early Archean oceanic crust was greater than the modern counterpart. It is generally accepted that the Archean mantle was hotter than today (e.g., Abbott et al., 1994). Hence, the higher heat flow due to the hot Archean mantle is considered to have been responsible for the high alteration temperature of the Early Archean oceanic crust.

6.3. Elemental Behavior During Alteration

Simple inspection of elemental concentrations is not satisfactory for the estimation of chemical exchange during alteration, because the concentrations of all elements are expressed as relative amounts. In this case, normalizing by highly immobile elements such as Al, Ti, and Zr is valid for determination of chemical changes (Gresens, 1967). Thus, we evaluate the chemical exchange of each element by using the enrichment factor calculated as following correction:

$$X^{\#} = (A_X/A_{TiO2})/(L_X/L_{TiO2}) \quad (4)$$

where $X^{\#}$ is the enrichment factor of element X, A_X is the concentration of element X in the altered sample, A_{TiO2} is the TiO_2 content of the altered sample, L_X is the average concentration of element X in the five least altered dolerites, and L_{TiO2} is the average TiO_2 content of the five least altered dolerites.

Figure 9 shows the average enrichment factor of each element in the altered dolerite, type I basalt, and type II basalt. In the altered dolerite, degrees of enrichment or depletion of all elements are relatively small. On the other hand, Na is noticeably depleted and K, CO_2, Rb, Ba, and U are significantly enriched in the type I and type II basalts, although the other elements show little departure from the line of one ($X^{\#} = 1$). The K-enrichment and Na-depletion probably reflect the replacement of plagioclase by K-mica. Rb and Ba are contained in the K-mica, leading to the $Rb^{\#}$-$K_2O^{\#}$ (Fig. 10a) and $Ba^{\#}$-$K_2O^{\#}$ (Fig. 10b) correlations. The type I and type II basalts are remarkably enriched in CO_2, reflecting the presence of carbonate minerals. The enrichment of U is also recognized in both type I and type II (Fig. 9b, c). However, the U concentrations do not correlate with any other element concentrations, and thus the cause of the U enrichment is uncertain.

Whereas two samples of the least altered dolerite have CO_2 contents of ~0.1 wt.% which is similar to that of modern fresh MORB (e.g., Humphris et al., 1980), one sample has relatively high CO_2 content of ~1 wt.%. Hence, there is significant variability in the CO_2 contents of the least altered dolerite (>100% relative standard deviation), as shown in Figure 9. However, it is reasonably considered that hydrothermal carbonatization is responsible for this high CO_2 content in the one sample, and the primary CO_2 content of the dolerite is close to 0.1 wt.%. The CO_2 contents in the basalt samples are well correlated with CaO contents (Fig. 11a), and the CaO/CO_2 ratios of the basalt are almost identical to that of pure calcite. This indicates that the carbonate minerals in the whole-rock basalt samples are predominantly calcite, and a relative contribution of ankerite and siderite to bulk-rock chemistry is trivial. Moreover, the regression line of the basalt data intersects the origin, indicating that almost all Ca exists as calcite. These results suggest that Ca in the primary igneous minerals and glass was completely redistributed to calcite, although Fe and Mg were mainly redistributed to the secondary silicates and sulfides such as chlorite and pyrite. Compared to the least altered dolerite that is relatively fresh and noncarbonatized, the average basalt is significantly enriched in CO_2 (Fig. 11b), reflecting the formation of calcite. On the other hand, the average $CaO^{\#}$ content of basalt is approximately the same as that of the least altered dolerite (Fig. 11b). This indicates that the CO_2 was trapped as calcite by using the Ca originally contained in the basalt, and that there was essentially neither gain nor loss of Ca during the hydrothermal carbonatization. The basalt average (solid star in Fig. 11b) does not contain

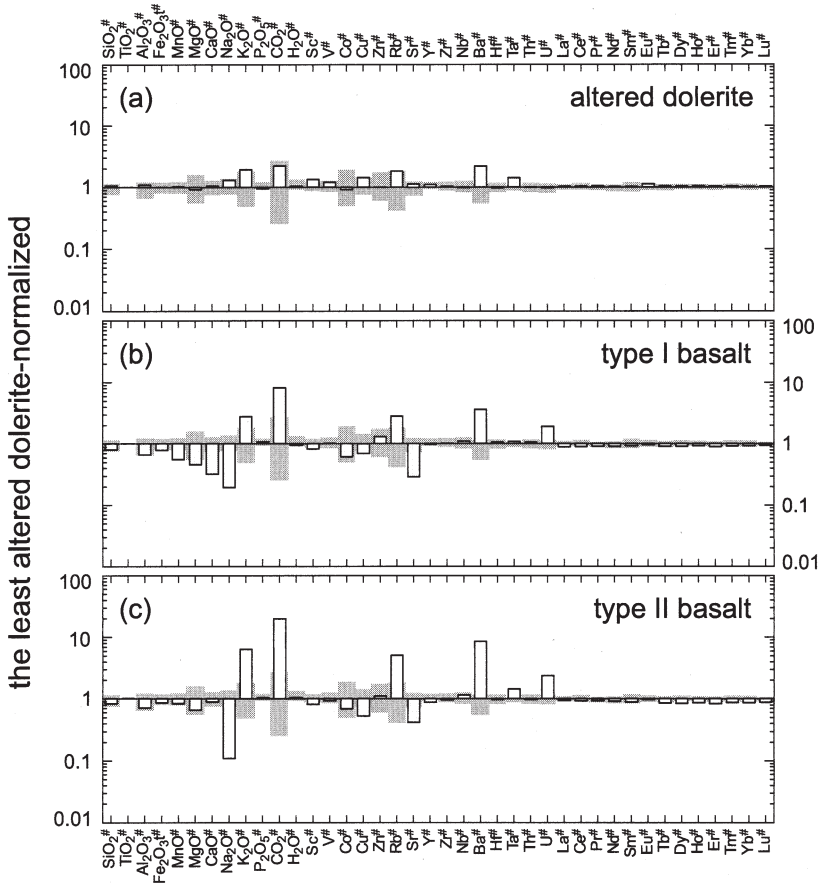

Fig. 9. Bar chart showing average enrichment factors of (a) altered dolerite, (b) type I basalt, and (c) type II basalt. Values >1 indicate addition and vice versa. Shaded areas represent the compositional range of the least altered dolerite. Fe_2O_3t = total iron as Fe_2O_3. Hash marks (#) designate enrichment factor of each element.

interpillow carbonate, which is probably responsible for slight depletion of $CaO^{\#}$ in the basalt average relative to the least altered dolerite.

Chemical exchange between seawater and oceanic crust by seafloor hydrothermal alteration is one of major factors to control ocean chemistry (Holland, 1984). Hydrothermally altered oceanic crust is well known as an important sink of Mg in the modern ocean system. This Mg-uptake is balanced to the leaching of Ca from the oceanic crust (e.g., Mottl and Holland, 1978). That is, Mg in the circulating hydrothermal fluid (originated from seawater) is trapped into the altered oceanic crust as Mg-rich secondary minerals (mainly chlorite), and Ca in the Ca-bearing minerals (e.g., plagioclase, clinopyroxene) and glass are compensatively dissolved into the hydrothermal fluid (finally into the ocean). This chemical exchange leads to the negative correlation between Ca and Mg in the modern altered oceanic crust. In contrast, there is no correlation between Ca and Mg contents in the Early Archean altered oceanic crust. Almost all Ca was retained as calcite in the Archean crust due to the hydrothermal carbonatization under the high-μCO_2 condition, and then the release of Ca into the ocean did not take place. This may be partly responsible for the lack of Mg-uptake in the Early Archean oceanic crust.

It is also well known that some alkaline elements (e.g., K, Rb, and Ba) are largely leached from the modern oceanic crust during high-temperature hydrothermal alteration (e.g., Seyfried and Mottl, 1982; Alt et al., 1996). In striking contrast, K, Rb, and Ba are significantly enriched in the Early Archean altered oceanic crust. These geochemical features are attributed to the replacement of plagioclase by K-mica. K, Rb, and Ba in the circulating hydrothermal fluid (seawater) were trapped into the altered basalt, whereas Na in the basalt was discharged into the fluid through the K-mica formation. As mentioned previously, it is considered that the high-μCO_2 condition of the hydrothermal fluid led to the formation of K-mica. Alternatively, the lower Mg/K of the Early Archean fluid than modern seawater may have promoted the formation of K-mica rather than chlorite, because the stability of K-mica versus chlorite depends on the Mg/K of the fluid. In either case, the Early Archean seafloor hydrothermal alteration was not only the cause of the unique fluid chemistry (e.g., high μCO_2, low Mg/K), but also the consequence for coeval ocean chemistry (e.g., Mg/Ca, K/Na).

6.4. Significance of MOR Hydrothermal Alteration for the Early Archean Global Carbon Cycle

Our geological and geochemical lines of evidence suggest that the Early Archean oceanic crust was hydrothermally car-

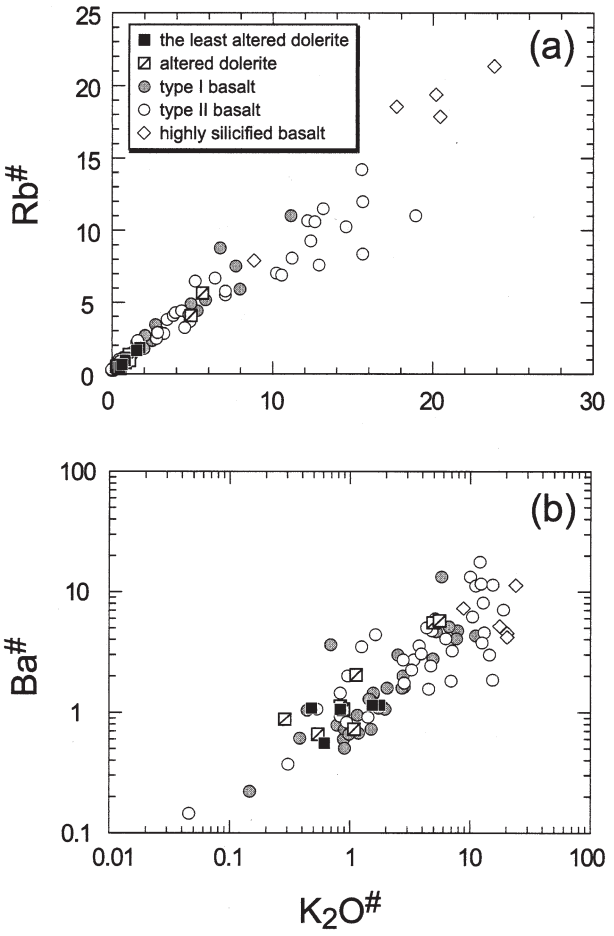

Fig. 10. Enrichment factors for (a) K_2O vs. Rb and (b) K_2O vs. Ba for dolerite and basalt. Hash marks (#) designate enrichment factor of each element.

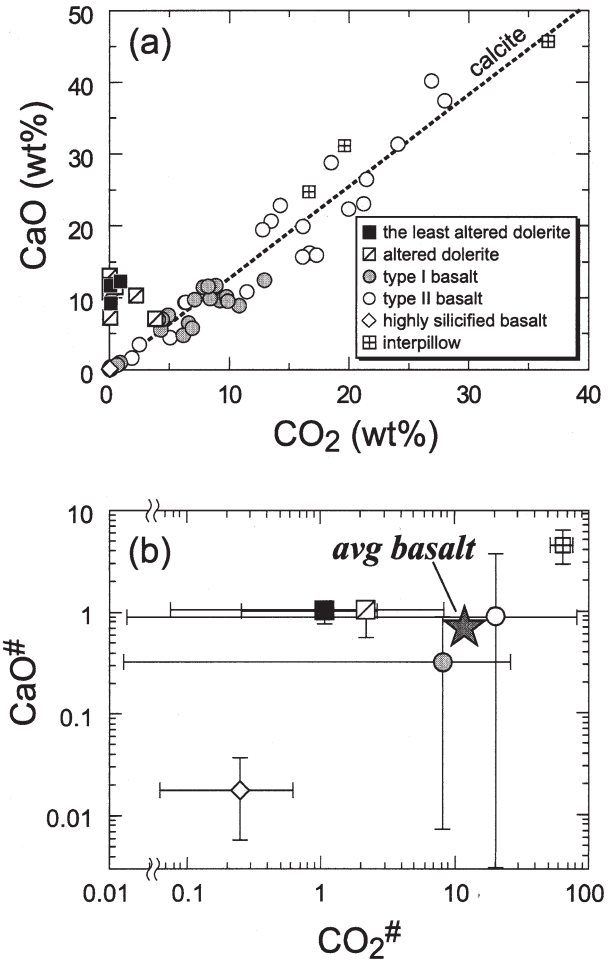

Fig. 11. (a) CO_2 vs. CaO for dolerite, basalt, and interpillow material. Dashed bold line represents CaO/CO_2 ratio of pure calcite; (b) enrichment factors for CO_2 vs. CaO for dolerite, basalt, and interpillow material. Symbols and solid lines represent mean values and ranges, respectively. Solid star represents the mean value of type I, type II, and highly silicified basalts. Hash marks (#) designate enrichment factor of each element.

bonatized by the reaction between Ca in the basalt and CO_2 in the circulating CO_2-rich seawater. To assess the significance of the hydrothermal carbonatization for the Early Archean global carbon cycle, we estimate the carbon flux sunk into the oceanic crust. The carbon flux can be estimated by multiplying the content of carbon trapped in the oceanic crust by the production rate of altered oceanic crust as:

$$F_C = C_C R_{cc} \quad (5)$$

where F_C is the carbon flux into the oceanic crust (mol/yr), C_C is the average carbon content of altered oceanic crust (mol/g), and R_{cc} is the production rate of the carbonatized oceanic crust (g/yr). The R_{cc} can be further estimated by:

$$R_{cc} = sp\ D_{cz}\ \rho_{ba} \quad (6)$$

where sp is the spreading rate of oceanic crust (cm^2/yr), D_{cz} is the depth of carbonatized zone (cm), and ρ_{ba} is the density of oceanic crust (g/cm^3).

The C_C is given as the average carbon content of all basalt samples; 1.4×10^{-3} mol/g (as dolerite is a significantly minor component, the C_C does not include dolerite data). Carbonate carbon in microscopic veinlets and vesicles is included in the C_C, but the carbon in interpillow space is not included because the accurate evaluation of proportion of interpillow carbonate is very difficult. Hence, this C_C value is the minimum estimate. In the sampling area, total thickness of the tholeiitic basalt unit is 500m, and all basalt samples in the area were subject to hydrothermal alteration. The tholeiitic basalt horizon deeper than 500m is lost by the shearing of later-stage tectonic movement probably due to accretion (obduction). Thus, the depth of the hydrothermally carbonatized basalt unit must be greater than 500m. In fact, the larger depth of the Archean seafloor hydrothermal alteration (~1000m) has been reported from the North Pole Dome, Pilbara Craton (Kitajima et al., 2001), and the D_{cz} value of 500 m in the present study is considered to be minimum estimate. The ρ_{ba} is assumed to be the same as modern basalt (3.0 g/cm^3; Karato, 1983). The sp of the Archean oceanic crust has been estimated by several researchers. Hargraves (1986) demonstrated that the sp of the Archean oceanic crust was one order of magnitude greater than the modern rate of 3.4×10^{10} cm^2/yr (Parsons, 1982) based on the plausible

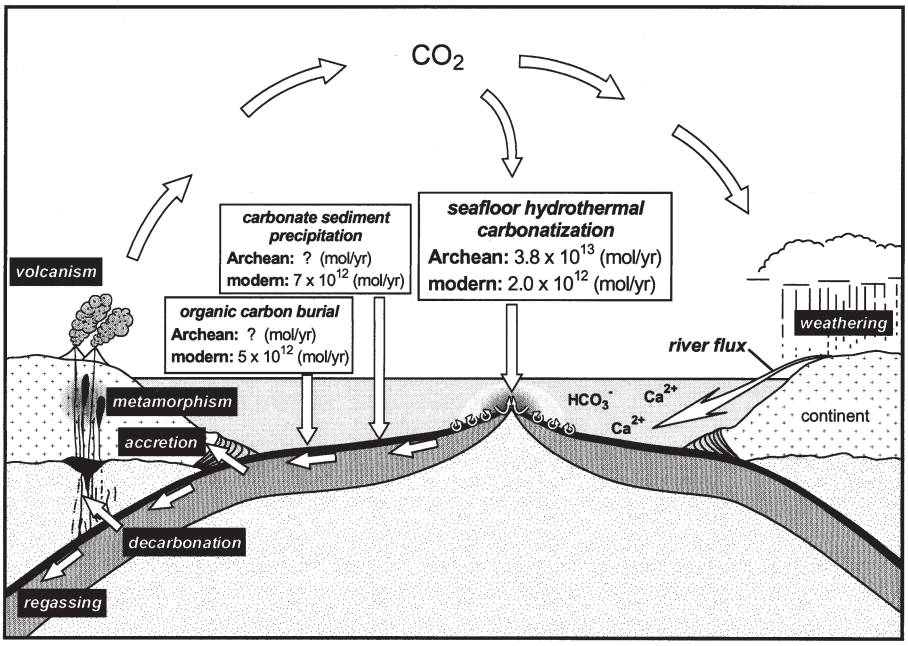

Fig. 12. Schematic illustration showing the global carbon cycle in the modern and Early Archean Earth together with the carbonate precipitation modes and estimated carbon fluxes. The carbon fluxes of carbonate sediment precipitation and organic carbon burial in the Early Archean are still uncertain, but these fluxes were very likely much smaller than today as the volume of continental crust and riverine flux were probably minor. The carbon fluxes of carbonate sediment precipitation, organic carbon burial, and submarine hydrothermal carbonatization in the modern Earth have been estimated by Berner (1991), Berner (1989), and Alt and Teagle (1999), respectively.

thermal condition of Archean mantle. In contrast, mantle degassing history constrained by the degassing rate of ^{40}Ar suggests that the spreading rate was approximately the same as the modern rate (Tajika and Matsui, 1993). For the sake of convenience, the mean value (1.8×10^{11} cm^2/yr) is used for our calculation, while the range of possible spreading rates leads to a 50% uncertainty in the flux. Although there are some uncertainties in spreading rate and the carbon content of altered basalts, we estimate the carbon flux into the Early Archean oceanic crust to be 3.8×10^{13} mol/yr.

A schematic illustration showing the carbon cycle model in the modern and Archean Earth is presented in Figure 12. In the modern Earth, carbon in the atmosphere and ocean is mainly fixed by carbonate sediment precipitation (7×10^{12} mol/yr; Berner, 1991) and organic carbon burial (5×10^{12} mol/yr, Berner, 1989). In addition, several authors have pointed out that low-temperature hydrothermal alteration of oceanic crust also fixes significant amounts of carbon (3.7×10^{12} mol/yr, Staudigel et al., 1989; 1.5–2.4 $\times 10^{12}$ mol/yr, Alt and Teagle, 1999). Therefore, the present-day total carbon sink (including the carbon flux associated with MOR hydrothermal alteration) is approximately 1.4×10^{13} mol/yr. In the Early Archean, the fluxes of carbonate sediment precipitation and organic carbon burial are unresolved, because there are great uncertainties in many constraints (e.g., continental volume, biologic productivity). Our estimation demonstrates that the carbon flux into the Early Archean oceanic crust by seafloor hydrothermal alteration was equivalent to or greater than the present-day total carbon flux. In addition to the MOR hydrothermal alteration, arc-related volcanic rocks of the Early Archean were severely subject to carbonatization (Barley, 1993). Therefore, total carbon flux by the seafloor hydrothermal carbonatization may be greater than our estimation. In either case, it is concluded that seafloor hydrothermal carbonatization played a major role as a CO_2 sink in the Early Archean global carbon cycle.

The carbonatized oceanic crust was partly accreted to continents (island-arcs) and was partly subducted into the mantle. The accreted carbonatized oceanic crust probably contributed to the decrease of atmospheric and oceanic CO_2 in the Early Archean, because the residence time of the accreted carbonatized crust in the global carbon cycle is extremely long (probably greater than the order of 10^9 yr because remnants of the Early Archean carbonatized oceanic crust are available at present). It is reasonably considered that the volume of accreted crust was significantly larger due to the subduction/obduction of young (buoyant) oceanic crust and longer convergent plate boundaries in the Early Archean than today (Hargraves, 1986).

Some parts of the carbonate carbon in the subducted altered oceanic crust were decarbonated and then returned to the atmosphere through the mantle wedge and continental (island-arc) crust. In addition, the degassed carbon may have influenced the geochemical processes in the mantle wedge related to the formation of the tectosphere. Quite recently, it has been revealed that carbonate minerals contained in altered oceanic crust are only slightly decarbonated during the subduction process on the modern Earth, and hence are regassed into deeper mantle than previously thought (Kerrick and Connolly, 2001). On the other hand, the degree of decarbonation of the Archean carbonatized crust through subduction may have been higher, due to the hotter potential mantle temperature, greater

by 150 to 200°C than today (Abbott et al., 1994; Komiya, 2001). Thus it is inferred that the fraction of regassing of carbonate carbon into mantle along Archean subduction zones was much smaller than today. Based on a model calculation, however, Sleep and Zahnle (2001) evaluated that even a small fraction (~0.2) of regassed carbonate carbon from altered oceanic crust could be effective for the decrease of atmospheric and oceanic CO_2. We believe that carbonatization of oceanic crust by seafloor hydrothermal alteration, subsequent accretion of the carbonatized oceanic crust, and possible regassing of the deep mantle by the carbonatized crust through subduction were among the most important geological processes for decreasing the atmospheric and oceanic CO_2 level in the Early Archean.

7. CONCLUSIONS

Detailed geological, petrological, and geochemical investigations of the Early Archean hydrothermally altered basaltic rocks from the Warrawoona Group provide the following conclusions:

1. Basaltic rocks from the study area are divided into basalt and dolerite. The dolerite is characterized by the alteration mineral assemblage of typical greenschist facies. On the other hand, the alteration mineral assemblage of basalt suggests that the basalt was altered by the hydrothermal fluid with high μCO_2.
2. The basaltic rocks were mainly subject to carbonatization. Geochemical and carbon isotopic data suggest that the carbonate minerals in the basalt were formed by the reaction between CO_2 in the circulating seawater and Ca in the oceanic crust.
3. The chemical flux of CO_2 sunk into the Early Archean oceanic crust is estimated to be 3.8×10^{13} mol/yr, based on the average carbon content of altered oceanic crust of 1.4×10^{-3} mol/g, the alteration depth of 500 m, and the spreading rate of 1.8×10^{11} cm^2/yr. The estimated CO_2 flux is equivalent to or greater than the present-day total carbon flux (~1.4×10^{13} mol/yr). The carbonatization of oceanic crust by the seafloor hydrothermal alteration acted as an important sink of atmospheric and oceanic CO_2 in the Early Archean.

Acknowledgments—We would like to thank Y. Watanabe and N. Imai for ICP-MS analysis, and H. Yoshida, T. Ishii, S. Haraguchi, H. Sato, and S. Machida for XRF and EPMA analyses. We also thank Y. Hamada for CO_2 determination, and A. Ueda, A. Kawabata, S. Unami, and S. Kataoka for carbon isotopic analysis. Field collaboration with S. Maruyama, M. Terabayashi, G. Kimura, Y. Isozaki, and T. Komiya was of great assistance. We have also benefited from discussions with H. D. Holland and H. Ohmoto. We also thank J. C. Alt (associate editor), N. H. Sleep, M. E. Barley, and an anonymous reviewer for helpful comments that significantly improved the manuscript. This work was supported by the Ministry of Education, Culture, Sports, Science and Technology of Japan through Grant-in-Aid Nos. 07238102, 06041038, 08041102, 06740415, 07740426, 11740295, 13440160, and 15204048 to YK, and 15–11211 to KN and by funds from cooperative programs to YK provided by the Ocean Research Institute, University of Tokyo.

Associate editor: J. Alt

REFERENCES

Abbott D. L., Burgess L., Longhi J., and Smith W. H. F. (1994) An empirical thermal history of the Earth's upper mantle. *J. Geophys. Res.* **99,** 13835–13850.

Alt J. C. and Teagle D. A. H. (1999) The uptake of carbon during alteration of oceanic crust. *Geochim. Cosmochim. Acta* **63,** 1527–1535.

Alt J. C., Laverne C., Vanko D. A., Tartarotti P., Teagle D. A. C., Bach W., Zuleger E., Erzinger J., Honnorez J., Pezard P. A., Becker K., Salisbury M. H., and Ewilkens R. H. (1996) Hydrothermal alteration of a section of upper oceanic crust in the eastern equatorial pacific: a synthesis of results from Site 504 (DSDP Legs 69, 70, and 83, and ODP Legs 111, 137, 140, and 148). *Proc. ODP, Sci. Results* **148,** 417–434.

Arndt N. T., Nelson D. R., Compston W., Trendall A. F., and Thorne A. M. (1991) The age of the Fortescue Group, Hamersley basin, Western Australia, from ion microprobe zircon U–Pb results. *Aust. J. Earth Sci.* **38,** 261–281.

Barley M. E. (1993) Volcanic, sedimentary and tectonostratigraphic environments of the ~3.46Ga Warrawoona Group: A review. *Precamb. Res.* **60,** 47–67.

Barley M. E. and Groves D. I. (1987) Hydrothermal alteration of Archaean supracrustal sequences in the central Norseman-Wiluna Belt, Western Australia: A brief review. *Geol. Dept. and Univ. Extension, Univ. West. Aust. Publ.* **11,** 51–66.

Barley M. E. and Pickard A. L. (1999) An extensive, crustally-derived, 3325 to 3310 Ma silicic volcanoplutonic suite in the eastern Pilbara Craton: Evidence from the Kelly Belt, McPhee Dome and Corunna Downs Batholith. *Precamb. Res.* **96,** 41–62.

Berner R. A. (1989) Biogeochemical cycles of carbon and sulfur and their effect on atmospheric oxygen over Phanerozoic time. *Palaeogeogr. Palaeoclimat. Palaeocol.* **75,** 97–112.

Berner R. A. (1991) A model for atmospheric CO_2 over Phanerozoic time. *Am. J. Sci.* **291,** 339–376.

Berner R. A., Lasaga A. C., and Garrels R. M. (1983) The carbonate-silicate geochemical cycle and its effect on atmospheric carbon dioxide over the past 100 million years. *Am. J. Sci.* **283,** 641–683.

Bottinga Y. (1969) Calculated fractionation factors for carbon and hydrogen isotope exchange in the system calcite-CO_2-graphite-methane-hydrogen and water vapor. *Geochim. Cosmochim. Acta* **33,** 49–64.

Burrows D. R., Wood P. C., and Spooner E. T. C. (1986) Carbon isotope evidence for a magmatic origin for Archean gold-quartz vein ore deposits. *Nature* **321,** 851–854.

Cameron E. M. and Hattori K. (1987) Archean gold mineralization and oxidized hydrothermal fluids. *Econ. Geol.* **82,** 1177–1191.

Condie K. C. (1994) Greenstones through time. In *Archean Crustal Evolution* (ed. K. C. Condie), pp. 85–120, Elsevier.

Condie K. C. (1997) *Plate Tectonics and Crustal Evolution.* 4th ed, Butterworth-Heinemann.

Criss R. E. (1995) Stable isotope distribution: Variations from temperature, organic and water-rock interactions. In *Global Earth Physics-A Handbook of Physical Constraints* (ed. J. A. Thomas), AGU Reference Shelf 1, pp. 292–307, American Geophysical Union, Washington, DC.

de Wit M. J. and Hart R. A. (1993) Earth's earliest continental lithosphere, hydrothermal flux and crustal recycling. *Lithos.* **30,** 309–335.

Ferguson K. M. and Ruddock I. (2001) Mineral occurrences and exploration potential of the East Pilbara. *Geol. Surv. West. Aust., Rep.* **81,** 114 p.

Golding S. D., Groves D. I., McNaughton N. J., Barley M. E., and Rock N. M. S. (1987) Carbon isotopic composition of carbonates from contrasting alteration styles in supracrustal rocks of the Norseman-Wiluna Belt, Yilgarn Block, Western Australia: Their significance to the source of Archaean auriferous fluids. *Geol. Dept. and Univ. Extension, Univ. West. Aust. Publ.* **11,** 215–238.

Green M. G., Sylvester P. J., and Buick R. (2000) Growth and recycling of early Archaean continental crust: Geochemical evidence from the Coonterunah and Warrawoona Groups, Pilbara Craton, Australia. *Tectonophysics* **322,** 69–88.

Gresens R. L. (1967) Composition-volume relations of metasomatism. *Chem. Geol.* **2,** 47–65.

Groves D. I., Golding S. D., Rock N. M. S., Barley M. E., and McNaughton N. J. (1988) Archean carbon reservoirs and their relevance to fluid source for gold deposits. *Nature* **331,** 254–257.

Hargraves R. B. (1986) Faster spreading or greater ridge length in the Archean? *Geology* **14,** 750–752.

Heydari E., Wade W. J., and Hassanzadeh J. (2001) Diagenetic origin of carbon and oxygen isotope compositions of Permian-Triassic boundary strata. *Sed. Geol.* **143,** 191–197.

Hickman A. H. (1983) Geology of the Pilbara Block and its Environs. *Geol. Surv. West. Aust. Bull.* **127,** 268 p.

Hofmann A. W. (1988) Chemical differentiation of the Earth: The relationship between mantle, continental crust, and oceanic crust. *Earth Planet. Sci. Lett.* **90,** 297–314.

Holland H. D. (1984) *The Chemical Evolution of the Atmosphere and Oceans.* Princeton University Press.

Humphris S. E., Thompson R. N., Gibson I. L., and Marriner G. (1980) Comparison of geochemistry of basalts from the East Pacific Rise, OCP Ridge, and Siqueiros Fracture Zone, Deep Sea Drilling Project Leg 54. *Init. Repts. DSDP* **54,** 635–649.

Imai N. (1990) Multielement analysis of rocks with the use of geological certified reference material by inductively coupled plasma mass spectrometry. *Anal. Sci.* **6,** 389–395.

Karato S. (1983) Physical properties of basalts from Deep Sea Drilling Project Hole 504B, Costa Rica Rift. *Init. Repts. DSDP* **69,** 687–695.

Kasting J. F. (1987) Theoretical constraints on oxygen and carbon-dioxide concentrations in the Precambrian atmosphere. *Precamb. Res.* **34,** 205–229.

Kasting J. F. (1993) Earth's early atmosphere. *Science* **259,** 920–926.

Kato Y. and Nakamura K. (2003) Origin and global tectonic significance of Early Archean cherts from the Marble Bar greenstone belt, Pilbara Craton, Western Australia. *Precamb. Res.* **125,** 191–243.

Kato Y., Ohta I., Tsunematsu T., Watanabe Y., Isozaki Y., Maruyama S., and Imai N. (1998) Rare earth element variations in mid-Archean banded iron formations: Implications for the chemistry of ocean and continent and plate tectonics. *Geochim. Cosmochim. Acta* **62,** 3475–3497.

Kato Y., Nakao K., and Isozaki Y. (2002) Geochemistry of Late Permian to Early Triassic pelagic cherts from southwest Japan: Implications for an oceanic redox change. *Chem. Geol.* **182,** 15–34.

Kerrick D. M. and Connolly J. A. D. (2001) Metamorphic devolatilization of subducted oceanic metabasalts: Implications for seismicity, arc magmatism and volatile recycling. *Earth Planet. Sci. Lett.* **189,** 19–29.

Kishida A. and Kerrich R. (1987) Hydrothermal alteration zoning and gold concentration at the Kerr-Addison Archean lode gold deposit, Kirkland Lake, Ontario. *Econ. Geol.* **82,** 649–690.

Kitajima K., Maruyama S., Utsunomiya S., and Liou J. G. (2001) Seafloor hydrothermal alteration at an Archaean min-ocean ridge. *J. Metamorphic Geol.* **19,** 581–597.

Knauth L. P., Brilli M., and Klonowski S. (2003) Isotope geochemistry of caliche developed on basalt. *Geochim. Cosmochim. Acta* **67,** 185–195.

Komiya T. (2001) Secular change of the composition and temperature of the upper mantle. In *Proceedings of the Extended Abstracts of 4th International Archean Symposium* (eds. K. F. Cassidy et al.), pp. 54–56, AGSO-Geoscience Australia Record 2001/37.

Krishnamurthy R. V., Schmitt D., Atekwana E. A., and Baskaran M. (2003) Isotopic investigations of carbonate growth on concrete structures. *Appl. Geochem.* **18,** 435–444.

Maruyama S., Isozaki Y., and Kimura G. (1991) Is the Mid-Archean barite formation from the Pilbara Craton, Australia, under the deep-sea environment? *EOS Trans. Am. Geophys. Union* **72,** 532.

Masuda A. (1975) Abundances of monoisotopic REE, consistent with the Leedey chondrite values. *Geochem. J.* **9,** 183–184.

Masuda A., Nakamura N., and Tanaka T. (1973) Fine structures of mutually normalized rare-earth patterns of chondrites. *Geochim. Cosmochim. Acta* **37,** 239–248.

McNaughton N. J., Compston W., and Barley M. E. (1993) Constraints on the age of the Warrawoona Group, eastern Pilbara Block, Western Australia. *Precamb. Res.* **60,** 69–98.

Miyashiro A. (1994) *Metamorphic Petrology*, University College London Press, London, 404 p.

Mottl M. J. and Holland H. D. (1978) Chemical exchange during hydrothermal alteration of basalt by seawater-I. Experimental results for major and minor components of seawater. *Geochim. Cosmochim. Acta* **42,** 1103–1115.

Parsons B. A. (1982) Causes and consequences of the relation between the area and age of the ocean floor. *J. Geophys. Res.* **87,** 289–302.

Pavlov A. A., Kasting J. F., Brown L. L., Rages K. A., and Freedman R. (2000) Greenhouse warming by CH_4 in the atmosphere of early Earth. *J. Geophys. Res.* **105,** 11981–1.

Phillips G. N. (1986) Geology and alteration in the Golden Mile, Kalgoorlie. *Econ. Geol.* **81,** 779–808.

Ronov A. B. (1964) Common tendencies in the chemical evolution of the earth's crust, ocean and atmosphere. *Geokhimiya* **1964,** 715–743.

Ronov A. B. and Yaroshevsky A. A. (1967) Chemical structure of the earth's crust. *Geochemistry* **11,** 1041–1066.

Ronov A. B. and Yaroshevsky A. A. (1969) Chemical composition of the Earth's crust. In *The Earth's Crust and Upper Mantle* (ed. P. J. Hart), Geophys. Monogr. **13,** 37–57. American Geophysical Union, Washington, DC.

Rye R., Kuo P. H., and Holland H. D. (1995) Atmospheric carbon dioxide concentrations before 2.2 billion years ago. *Nature* **378,** 603–605.

Seki Y. (1973) Metamorphic facies of propylitic alteration. *J. Geol. Soc. Japan* **79,** 771–780.

Seyfried W. E. Jr. and Mottl M. J. (1982) Hydrothermal alteration of basalt by seawater under seawater-dominated conditions. *Geochim. Cosmochim. Acta* **46,** 985–1002.

Sleep N. H. and Zahnle K. (2001) Carbon dioxide cycling and implications for climate on ancient Earth. *J. Geophys. Res.* **106,** 1373–1399.

Staudigel H., Hart S. R., Schmincke H. U., and Smith B. M. (1989) Cretaceous ocean crust at DSDP Sites 417 and 418: Carbon uptake from weathering versus loss by magmatic outgassing. *Geochim. Cosmochim. Acta* **53,** 3091–3094.

Sun S. -S. and McDonough W. F. (1989) Chemical and isotopic systematics of oceanic basalts: Implications for mantle composition and processes. *Geol. Soc. Spec. Publ. London* **42,** 313–345.

Tajika E. and Matsui T. (1992) Evolution of terrestrial proto-CO_2-atmosphere coupled with thermal history of the Earth. *Earth Planet. Sci. Lett.* **113,** 251–266.

Tajika E. and Matsui T. (1993) Evolution of seafloor spreading rate based on ^{40}Ar degassing history. *Geophys. Res. Lett.* **20,** 851–854.

Thompson A. B. (1971) P_{CO2} in low-grade metamorphism; zeolite, carbonate, clay mineral, prehnite relations in the system CaO-Al_2O_3-SiO_2-CO_2-H_2O. *Contrib. Mineral. Petrol.* **33,** 145–161.

Thorpe R. I., Hickman A. H., Davis D. W., Mortensen J. K., and Trendall A. F. (1992) U-Pb zircon geochronology of Archean felsic units in the Marble Bar region, Pilbara Craton, Western Australia. *Precamb. Res.* **56,** 169–189.

Van Kranendonk M. J., Hickman A. H., Williams I. R., and Nijman W. (2001) Archaean Geology of the East Pilbara Granite-Greenstone Terrane Western Australia-A Field Guide. *Geol. Surv. West. Aust. Rec.* 2001/9, 134 p.

Veizer J., Hoefs J., Ridler R. H., Jensen L. S., and Lowe D. R. (1989) Geochemistry of Precambrian carbonates: I. Archean hydrothermal systems *Geochim. Cosmochim. Acta* **53,** 845–857.

Walker J. C. G., Hays P. B., and Kasting J. F. (1981) A negative feedback mechanism for the long-term stabilization of Earth's surface temperature. *J. Geophys. Res.* **86,** 9776–9782.

Zen E. (1961) The zeolite facies: An interpretation. *Am. J. Sci.* **259,** 401–409.